

© 2016 IEEE. Personal use of this material is permitted. Permission from IEEE must be obtained for all other uses, in any current or future media, including reprinting/republishing this material for advertising or promotional purposes, creating new collective works, for resale or redistribution to servers or lists, or reuse of any copyrighted component of this work in other works.

Digital Object Identifier (DOI): 10.1109/TPEL.2021.3064302.

IEEE Transactions on Power Electronics

A Comprehensive Assessment of Multiwinding Transformer-Based DC-DC Converters

Thiago Pereira
Felix Hoffmann
Rongwu Zhu
Marco Liserre

Suggested Citation

T. Pereira, F. Hoffmann, R. G. Zhu and M. G. Liserre, "A Comprehensive Assessment of Multiwinding Transformer-Based DC-DC Converters," in IEEE Transactions on Power Electronics (early access), DOI: 10.1109/TPEL.2021.3064302.

A Comprehensive Assessment of Multiwinding Transformer-Based DC-DC Converters

Thiago Pereira, *Student Member, IEEE*, Felix Hoffmann, *Student Member, IEEE*, Rongwu Zhu, *Member, IEEE*, and Marco Liserre, *Fellow, IEEE*

Abstract—Multiwinding-Transformer-based (MTB) DC-DC converter did emerge in the last 25 years as an interesting possibility to connect several energy systems and/or to offer higher power density because of the reduction of transformer core material and reduction of power converter stages. MTB DC-DC converters can be considered as an interesting compromise between non-modular and a modular DC-DC converter since they are themselves modular in the construction. This eventually leads to some fault-tolerant possibilities since the multiwinding transformer (MWT) connects multiples ports and if one of them is not working anymore and it can be isolated, the others might still continue operating. Unfortunately, it is exactly the MWT that creates most of the technical challenges of this class of DC-DC converters because of the cross-coupling effects among the cells which make especially the resonant-topology very challenging to be designed. This paper reviews the history of the MTB DC-DC and then provides a classification of them, comparing them with Figure of Merits (FOM) and focusing on which is the maximum possible number of windings and which are the most suited magnetic core types. The problems coming from cross-coupling and the possible fault-tolerant operation are analysed with the help of simulation and experimental results.

Index Terms—Active-Bridge, DC-DC Converter, Fault-Tolerant, Multiwinding Transformer, Modular Converters

I. INTRODUCTION

IN the last three decades, several isolated DC-DC converter topologies have been widely investigated in the literature for integrating distributed DC power sources, storage units, and DC loads, enhancing the power transfer capability and increasing the conversion efficiency [1]–[5]. However the isolated multiport DC-DC converters, in particular, those based on the MWT have been drawn more attention [6]–[20], due to their advantages in the applications where multiple DC sources and/or loads should be integrated, while ensuring galvanic isolation and adopting different voltage levels among the ports.

In the literature, the MWT was first introduced as the key element of a multiple-output DC-DC converter by [6] in 1970s. In this converter, the concept based on the cross-regulation (proposed in [21] for a three-winding transformer) was used to ensure the adjustment of the output voltages through the magnetic coupling. Afterwards, in 1990s by [22], the same

concept employing also MWT was extended to a multiple-input DC-DC converter, whereas the first electrical model of MWT was being developed by [23].

Years later, in 2000s, to overcome the control limitations of the prior topologies, an unidirectional three-ports DC-DC converter using a three-winding transformer was introduced by [7] for integrating multiple DC sources individually and simultaneously to a single load. Then, based on this work, a bidirectional four-ports version employing a four-winding transformer and a family of multiport bidirectional DC-DC converters were proposed by [8] and [9], respectively.

Derived from the dual-active-bridge (DAB), in [9]–[12], the triple-active-bridge (TAB) was introduced with the same aim of integrating simultaneously multiple DC sources and loads. Concurrently, a three-port version of the series-resonant (SR) converter was introduced by [24]. However, only in [13], [14], the TAB and QAB converters were generalized for an arbitrary number of coupled cells with the called multiple-active-bridge (MAB). Finally, other papers have gradually arisen in the literature to further investigate these converters in several application fields, e.g. solid-state transformer (SST), electric vehicles (EVs), hybrid grids, and DC networks [15]–[20].

As there are hundreds of possible topologies for multiport converters based on MWT and their potentials and challenges have so far not been fully covered in the literature, this paper proposes a novel class denoted MTB DC-DC converters. Unlike the classical modular converter based on multiple two-winding transformers (2WT), the MTB converters have more degrees of freedom in terms of architecture: symmetrical (equal number of cells in both side of the MWT) or asymmetrical (different number of cells in both side), which enlarge the opportunities in many application fields with different design requirements. Thus, derived in general from well-defined DC-DC converters (as DAB and SR), the MTB converters arise as promising solution of isolated and modular DC-DC converter, preserving similar characteristics. Nevertheless, the advantages and issues of each of them have not been thoroughly investigated yet in the literature.

In this context, the MTB converters are systematically addressed and evaluated in a generic approach, merging the topologies in categories regarding their architecture, resonant and non-resonant operation. Furthermore, an assessment and comparison are further addressed in terms of number of cells, power density, semiconductor technologies, power losses, cost and reliability. In this analysis, the classical modular solution based on multiples isolated DC-DC converters using 2WT is considered for sake of comparison. Thus, it is demon-

Manuscript received October 26, 2020; revised January 31, 2021; accepted February 27, 2021. Date of publication Month xx, 2021; date of current version Month xx, xxxx. Recommended for publication by Associate Editor xxxx. (Corresponding author: Thiago Pereira).

T. Pereira, F. Hoffmann, R. Zhu, and M. Liserre are with the Chair of Power Electronics, Christian Albrechts-University zu Kiel, Kiel 24118, Germany (e-mail: tp@tf.uni-kiel.de, fho@tf.uni-kiel.de, rzh@tf.uni-kiel.de and liserre@ieee.org).

strated that the number of cells and associated circuits can be decreased due to the magnetic coupling among the cells, reducing cost, size, and volume. As a result, this can lead to higher power density and efficiency.

However, the common magnetic core and its resulting coupling bring specific challenges depending on the number of windings and their arrangement. Thus, the impact of the undesired cross-coupling and the parameter deviation are highlighted and then a proper winding structure is proposed for different core geometries. Additionally, a fault-tolerant approach based on the MWT is introduced, taking into account the reconfiguration and continuous operation of the system even under a fault condition. Therefore, the main goal of this paper is to provide an overview of the MTB DC-DC Converters from the topology perspective, considering their potentials and challenges. The novelty arises from the explanation of these two points in a comprehensive way. As the final outcome, the main MTB topologies are quantitatively compared.

The paper is organized as follows: Section II shows an overview and classification of the MTB topologies. Section III introduces the potential and challenges of the MWT in MTB topologies, describing the MWT redundancy approach and its features to keep the continuous operation. Section IV presents the interconnection and operation modes issues. Section V shows the quantitative analysis among the MTB converter. Finally, the outcomes are presented in Section VI.

II. ARCHITECTURE AND OPERATION PRINCIPLE OF THE MTB DC-DC CONVERTERS

A. Generic Scheme of the MTB Topologies

A MTB DC-DC converter consists of several cells connected to the same MWT, as illustrated in Figure 1. In this modular architecture, the MWT performs an important role establishing the high-frequency magnetic coupling between the cells and consequently composing the modules and the overall power converter. Thus, the architecture of the MTB DC-DC converter can be generically defined by combining of:

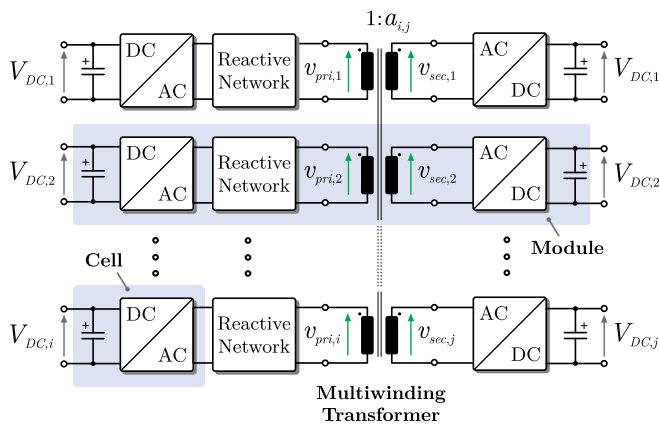


Figure 1. Generic scheme of the MTB topologies, consisting of different cells (switched network based on active, hybrid and passive bridges) coupled magnetically by using the MWT to compose the modules (building blocks) and then these modules are combined to create the entire system. Where $V_{DC,i}$ and $V_{DC,j}$ are the DC voltages, $v_{pri,i}$ and $v_{sec,j}$ are the AC voltages on each port of the MWT, and $a_{i,j}$ the turn-ratio.

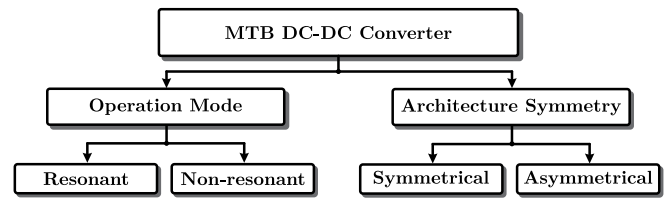


Figure 2. Generic classification of the MTB topologies.

i primary-side cells $N_{cells,pri}$ (whereas $i = 1, 2, \dots, N_{cells,pri}$); i reactive networks; j secondary-side cells $N_{cells,sec}$, (whereas $j = 1, 2, \dots, N_{cells,sec}$); and a MWT with the number of windings (N_w) divided in i and j ports (i.e. $N_w = i + j$) of turn-ratio $a_{i,j} = v_{sec,j}/v_{pri,i}$ (or $a_{i,j} = n_{sec,j}/n_{pri,i}$, where $n_{pri,i}$ is the number of turns on the i th primary-side cell and $n_{sec,j}$ on j th secondary-side cell).

It should be noted that the reactive network is represented in this paper as the combination of the primary side elements with the reflected ones, from the secondary side, in a single reactive network arranged by the equivalent elements. As can be seen, assuming a power flow from primary to the secondary side, the structure is composed firstly by an inverter stage (DC-AC stage) and then by a rectifier stage (AC-DC stage). In the middle, it is placed the MWT in series with the reactive network, which provides the resonant or non-resonant behavior for the DC-DC converter, depending on the arrangement of the reactive components: capacitor, leakage inductor (or an external inductor) and magnetizing inductance.

B. Classification of MTB DC-DC Topologies

In general, the MTB topologies can be classified according to its operation mode (such as resonant or non-resonant behavior), and according to its architecture symmetry (e.g. asymmetrical and symmetrical structure) as shown in Figure 2.

1) *Resonant and Non-resonant Operation Mode*: The reactive network is composed by reactive components and is used to modify the shapes of the switch current waveforms in order to define the resonant or non-resonant behavior of the power converter. Occasionally, these reactive elements are not necessarily required, since they will always be present in practice due to the inherent parasitic elements of the transformer (e.g. leakage/magnetizing inductances and capacitances). In this context, the SR, LLC (resonant) and DAB (non-resonant) converter have been used as a building block of the MTB topologies, because of their characteristics of soft-switching, high efficiency, and power density [9], [11], [12], [18].

The SR converter presents a well-regulated output voltage for a wide range of load, avoiding the requirement of close-loop control and also reducing the number of sensors. For that reason, SR converter is also denominated *DC transformer* [1], [17], [18]. Its reactive network is composed by a resonant capacitor connected in series to a resonant inductor. Reducing the ratio between the resonant and the magnetizing inductance of the transformer leads to the LLC converter, which enhances the voltage-control capability compared to SR converters [38].

When output voltage control or power-flow control is required, the DAB converter becomes a promising option,

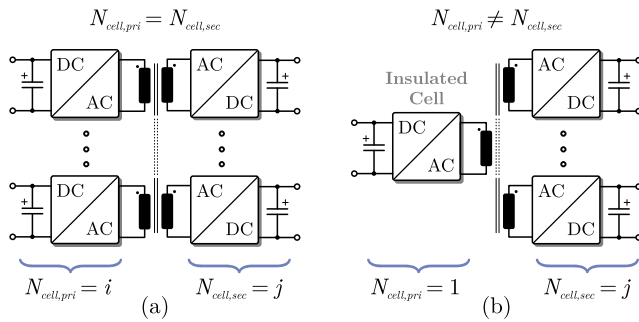


Figure 3. Architecture classification of the MTB topologies regarding the symmetry: (a) symmetrical configuration (i.e. $i = j$) and (b) asymmetrical configuration (i.e. $i < j$, with at least one cell $N_{cell,pri} = 1$), similarly its swapped version is also valid (i.e. $i > j$, with $N_{cell,sec} = 1$).

because it operates with active control of the power flow. The reactive network of the DAB is composed typically by a resonant inductor, which acts as a power transfer element between the cells. The amount of transferred power depends on the applied voltage across the reactive network and it is conventionally controlled by means of a phase-shift between these voltages. In some cases, the reactive network can also contain a capacitor to block the undesired DC component on the current, avoiding a saturation of the transformer.

2) *Architecture Symmetry*: Regarding the symmetry, MTB topologies can be classified as symmetric and asymmetric, depending on how the cells are coupled to the MWT. When configured symmetrically, the number of cells are equally divided in both sides of the MWT, i.e. $N_{cell,pri} = N_{cell,sec}$, [cf. Figure 3 (a)], or asymmetrically, where the cells are unequally coupled in one of the sides, i.e. $N_{cell,pri} \neq N_{cell,sec}$, so that $i > j$ or $i < j$), [cf. Figure 3 (b)]. As a matter of nomenclature, $N_{cells,i,j}$ will be used to represent generically the number of cells in one of the sides of the MWT, since the converter can be bidirectional, the definition of primary and secondary side depends only on the power flow direction. Thus, when $N_{cells,i,j} = 2$, it means that there are two cells in each sides of the MWT for symmetrical configuration (2 : 2) and two cells in only one side of MWT for asymmetrical configuration (1 : 2), or also the swapped structure (2 : 1).

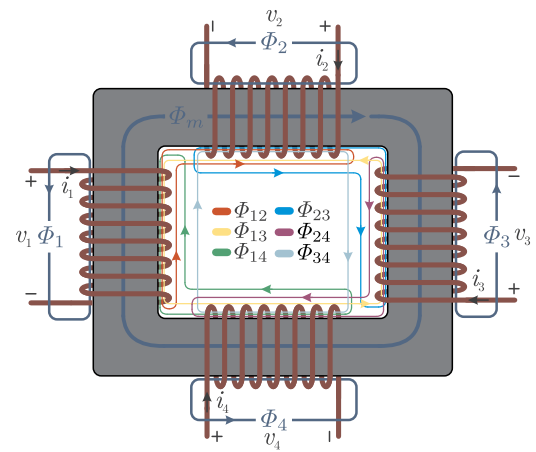


Figure 4. A MWT with four winding: the magnetic flux can be decomposed into the main flux, which links all the windings and is mainly confined inside the core, and leakage fluxes, which link only one or two of three windings.

C. Overview of the Main MTB DC-DC Converters

Considering the generic structure of the MTB DC-DC converters and the latest publications on the topic, an overview of the MTB topologies is gathered in Table I. As can be seen, the table merges the main MTB topologies based on the architecture symmetry along with different reactive networks.

III. ASSESSMENT AND COMPARATIVE ANALYSIS OF THE MTB DC-DC CONVERTERS

A. Potential of the MWT in MTB Topologies

Figure 4 illustrates a MWT with four windings. Each winding leads a current with a voltage applied on its terminals. The interaction of the currents and voltages result in a magnetic field. The magnetic flux in the field can be decomposed into: (i) main flux, Φ_m , which couple all the windings; (ii) self-leakage inductances, Φ_1 , Φ_2 , Φ_3 , and Φ_4 ; and (iii) mutual leakage inductances, Φ_{12} , Φ_{13} , Φ_{14} , Φ_{23} , Φ_{24} ; which couples two of the four windings as represented by their subscripts. As a result, the magnetic coupling allows the MTB topologies to integrate multiples sources/load of different power/voltage levels using fewer cells, cf. Figure 5 (a)-(c). In this context,

Table I
OVERVIEW OF THE MULTI-WINDING TRANSFORMER BASED TOPOLOGIES.

MTB DC-DC Converter	Architecture Symmetry	N ^o of Cells Pri : Sec	Operation Mode	Power Flow Pri ↔ Sec	Input/Output Cell	References
Triple-Active-Bridge (TAB)	Asymmetric	1 : 2	Non-resonant	Unidirectional	FB-SABR	[25]
				Bidirectional	FB-FWR	[26]
Quadruple-Active-Bridge (QAB)	Asymmetric	3 : 1	Non-resonant	Bidirectional	FB-FB	[10], [12], [27]–[29]
	Symmetric	2 : 2			FB-FB	[15], [18]–[20], [30], [31]
Penta-Active-Bridge (PAB)	Asymmetric	4 : 1	Non-resonant	Bidirectional	FB-FB	[18], [32], [33]
Multiple-Active-Bridge (MAB)	Symmetric	6 : 6	Non-resonant	Bidirectional	FB-FB	[34]
Three-Port LLC Converter	Asymmetric	1 : 2	Resonant	Bidirectional	HHB-FB	[37], [38]
					FB-FB	[39], [40]
Multiport LLC Converter	Symmetric	6 : 6	Resonant	Bidirectional	HHB/FB-FB	[41]
Three-Port SR Converter	Asymmetric	1 : 2	Resonant	Bidirectional	FB-FB	[24], [42], [43]

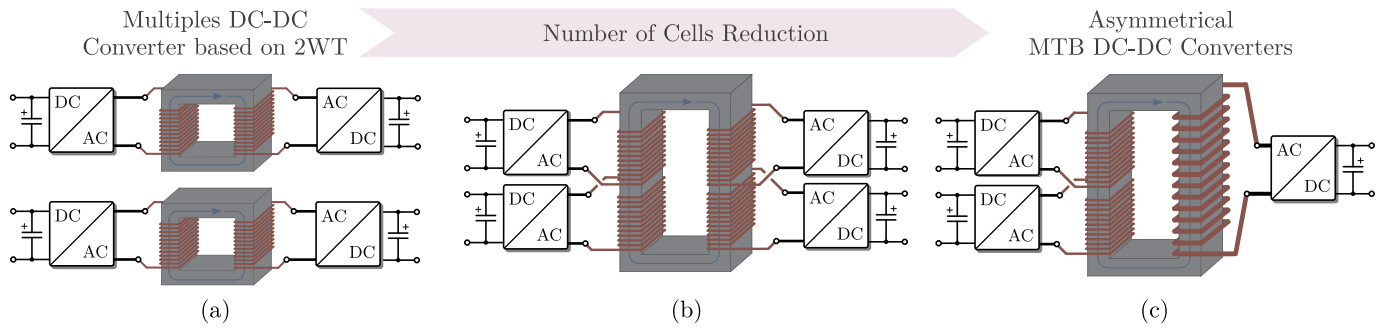


Figure 5. Comparison among the possible architectures: (a) using multiples 2WT; (b) MWT in symmetrical configuration and (c) MWT in asymmetrical. The reduction of the number cells in the asymmetrical configuration considering the same processed power is evident, since the windings can be merged in order to reduce the number of ports in one side of the MWT. As a matter of simplicity, it should be noticed that the reactive network was neglected.

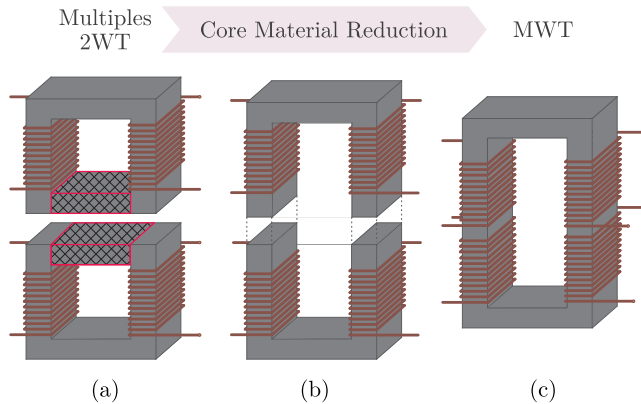


Figure 6. Comparison among the 2WT and MWT in terms of core material, highlighting graphically the material reduction using U-core, whereas: (a) multiple 2WTs with the potential reduction marked by the hatched region; (b) multiple 2WTs without the useless portion and (c) one MWT composed by means of multiple reduced 2WTs.

Table II
CORE MATERIAL REDUCTION BY USING THE MWT.

Magnetic Core Geometry	U-U	U-I	E-E	ETD-ETD
Core Material Reduction	10 %	15 %	12 %	2 %

based on the architecture symmetry, the symmetrical MTB (SMTB) topologies can be designed to merge its secondary-side cells in only one single cell, yielding then the asymmetrical MTB (AMTB) topologies and enabling also the reduction of cells, Figure 5 (c). As a result, the MTB DC-DC converter can provide advantages of reducing the cost and increasing power density, as described in detail next.

B. Power Density

Due to the magnetic coupling among the cells, the MWT presents a clear advantage regarding the material reduction compared to multiple 2WTs [cf. Figure 6]. As can be seen in Figure 6 (a), some core material can be saved when the 2WT is replaced by the MWT [cf. Figure 6 (b)-(c)], as listed in Table II for U-core, E-core, and ETD-core. Therefore, the concept of connecting magnetically the cells to compose the entire MTB DC-DC converter with MWT leads to benefits that can be demonstrated, using the 2WT in a conventional modular approach (i.e 2WT-based topologies), as reference. Thus, as a FOM, the area product A_p of a MWT [44], [45]

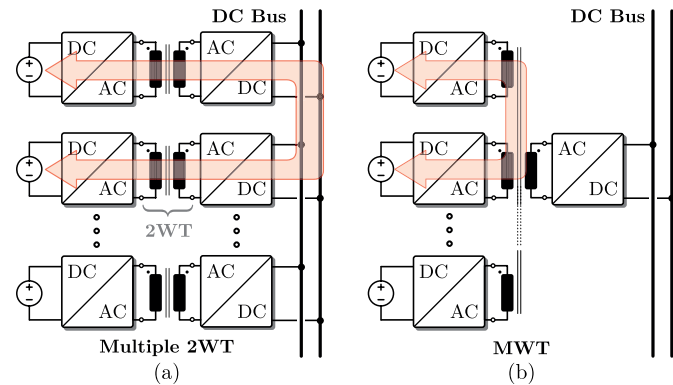


Figure 7. Interconnection among multiple DC sources (e.g PV system, storage system, super-capacitor and so on) considering systems based on: (a) multiple 2WTs and (b) one MWT.

[cf. (1)] can be used for deriving a scaling law, relating the volume of the MWT with the number of cells $N_{cells,pri}$ for any architecture (symmetrical or asymmetrical) [cf. Figure 3].

$$A_p = \frac{\sum_{k=0}^{i+j} (v_{rms,k})(i_{rms,k})}{K_f K_u f_{sw} J_{rms} \hat{B}} = \frac{S_T}{K_f K_u f_{sw} J_{rms} \hat{B}} \quad (1)$$

Where $v_{rms,k}$ is the applied rms voltage of the k th-winding, K_f is the form factor depending on the waveform shape, S_T is the total apparent power for a MWT with N_w windings, K_u is the core window utilization factor, f_{sw} is the switching frequency, J_{rms} is the rms current density and \hat{B} the peak value of the magnetic flux density.

Once the area product is proportional to the total apparent power S_T and also to the volume of the MWT V_{MWT} (i.e. $A_p \propto S_T \propto V_{MWT}$), they can be related to the processed power. Thus, in a simplified approach, the MWT can be considered a simple cube, so that $V_{MWT} \propto (S_T)^{\frac{3}{4}}$ [44], [46]. Assuming that 2WT is a particular design of MWT (i.e. $N_{cell,pri} = N_{cell,sec} = 1$), its volume can be expressed by $V_{2WT} = k_{Vol}(S_T)^{\frac{3}{4}}$, where k_{Vol} is the ratio between the core size of the 2WT and MWT (i.e. $0 < k_{Vol} \leq 1$).

For instance, considering the particular application, where multiple DC sources should be interconnected by means of a common DC bus, cf. Figure 7 (a)-(b). As can be noted, the power-paths between the sources can be shortened when the MWT is adopted, due to its inherent magnetic link, which

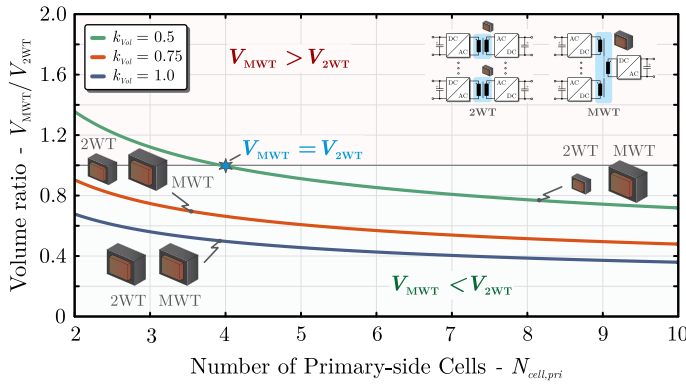


Figure 8. Volume ratio between the MWT and the equivalent association of multiple 2WTs (V_{MWT}/V_{2WT}) for the AMTB topologies with $N_{cell,pri}$ considering the core size used in 2WT equal to 50%, 75% and 100% of the MWT core size (i.e. $k_{Vol} = 0.5, 0.75,$ and 1.0).

allows the proper linkage without needing multiple conversion stages or even the common DC bus, cf. Figure 7 (a). As a result, since the structure uses less cells, the power density of the MTB topologies can be increased when the MWT is adopted, cf. Figure 7 (b). Therefore, assuming the all windings process the same power, the volume ratio between MWT and multiple 2WTs (N_{2WT}) can be expressed in terms of the number of sources (i.e. $N_{cell,pri}$), as defined in (2), which is valid only for $N_{cell,pri} \geq 2$.

$$\left. \frac{V_{MWT}}{V_{2WT}} \right|_{asym} = \frac{1}{k_{Vol} N_{2WT}} \left(\frac{N_{cell,pri} + 1}{2} \right)^{0.75} \quad (2)$$

Hence, as expected, the total MWT volume in asymmetrical configuration scales with the number of cells compared to multiple 2WT-based converters (cf. Figure 8). However, for the specific application, where the insulated cell of the AMTB topologies have to process the total power of the system, the MWT cannot be further scaled down, because the power processed by the windings of 2WT and MWT are the same (i.e. $S_{T,MWT} = S_{T,2WT}$), so that the A_p is nearly the same [cf. (1)]. Thus, for this kind of application, the only achievable reduction in the MWT is given by the fewer required amount of core material. Moreover, the MTB topologies are also composed by the cells, which have a significantly impact on the system volume and hence to the power density. Therefore, in order to evaluate their influence on the overall power density, the volume of the cells needs to be also defined.

Whereas the SMTB and 2WT-based topologies can be fully composed by $N_{cells,i,j}$ identical cells of volume $V_{o,cell}$, the AMTB topologies is composed by the same $N_{cells,i,j}$ cells and only one insulated cell which might has its volume $V_{o,icell}$ varying according to the total power processed. This means that $V_{o,icell}$ depends on several factor, such as topology and components adopted to implement this insulated cell (in particular power semiconductor and heat-sinks), and its design itself. Therefore, $V_{o,icell}$ can be generically derived by assuming two scenarios at a constant conversion efficiency ($\eta_{icell} = \eta_{cell}$). The first and best one, it is considered that the insulated cell is identical to the other cells, so that $V_{o,icell} = V_{o,cell}$ [cf. (3), where $k_{v,cell} = 1$]. In other words,

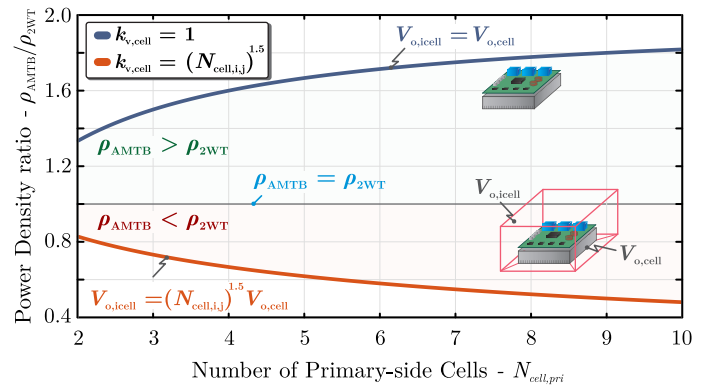


Figure 9. Power density ratio between the AMTB and 2WT-based topologies for the same power level considering the cells with the same volume and then the insulated cell with a volume proportional to the processed power.

the insulate is designed for achieving high-performance. The second and worst one, it is assumed that $V_{o,icell}$ is proportional to the processed power and hence to the number of cells [cf. (3), where $k_{v,cell} = (N_{cell,i,j})^{1.5}$].

$$V_{o,icell} = k_{v,cell} V_{o,cell}. \quad (3)$$

Based on both scenarios, the total volume of the different architectures can be derived as defined by (4), (5) and (6) (whereas $1 \leq k_{v,cell} \leq (N_{cell,i,j})^{1.5}$) for the 2WT-based converters, SMTB and AMTB topologies, respectively.

$$V_{Total,2WT} = 2N_{cell,i,j} V_{o,cell} + N_{cell,i,j} V_{2WT} \quad (4)$$

$$V_{Total,SMTB} = 2N_{cell,i,j} V_{o,cell} + V_{MWT} \quad (5)$$

$$V_{Total,AMTB} = (N_{cell,i,j} + k_{v,cell}) V_{o,cell} + V_{MWT} \quad (6)$$

Thus, as a FOM, (4) and (5) can be used for presenting the power density benefits and trade-offs of the AMTB topologies in comparison with 2WT-based ones, though the power density ratio, which is expressed by (7).

$$\frac{\rho_{AMTB}}{\rho_{2WT}} = \frac{2N_{cell,i,j} V_{o,cell} + N_{cell,i,j} V_{2WT}}{(N_{cell,i,j} + k_{v,cell}) V_{o,cell} + V_{MWT}} \quad (7)$$

By assuming the worst scenario in which the total volume of the transformers are equal (i.e. $V_{MWT} = N_{cell,i,j} V_{2WT}$), (7) can be used to find the upper and lower boundary of the power density ratio (ρ_{AMTB}/ρ_{2WT}), as depicted in Figure 9. As can be seen, the AMTB can be potentially advantageous when the volume of the insulated cell does not differ much from the other cells. In the practice, it means that the optimal set of topology, power semiconductor, and the number of cells should be considered for ensuring the best power density and then overcoming the high volume, due to the higher currents.

C. Design Considerations of the Insulated Cell

From Figure 9, it is noted that the performance of the AMTB topologies might be reduced when the number cells increase and hence the insulated cell has to process more power. However, its performance can be significantly improved when the topology and semiconductor technology are well selected. Depending on the power requirements, the conversion

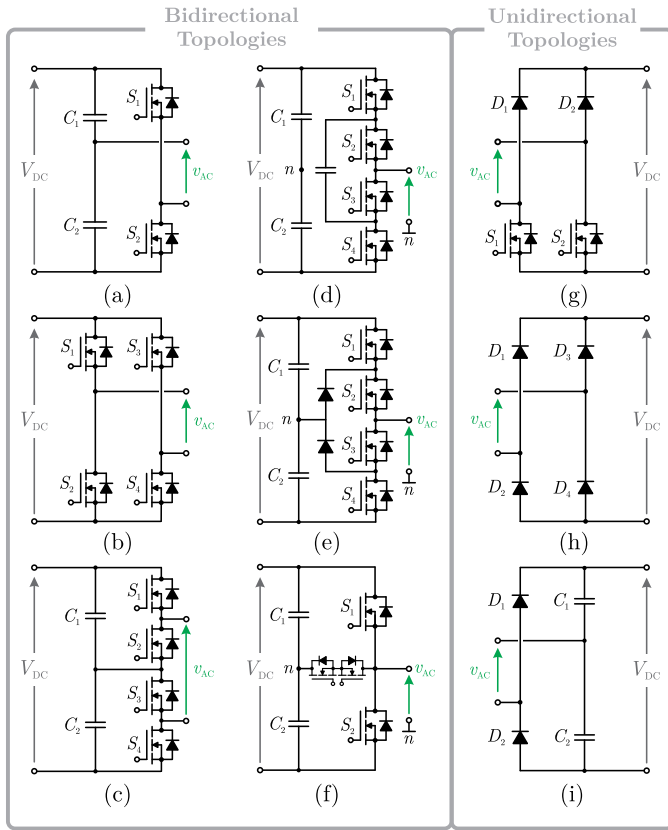


Figure 10. Main bidirectional topologies employed to implement the active cells of the MTB DC-DC converter: (a) Hybrid Half-bridge (HHB); (b) Full-bridge (FB); (c) Three-level bridge (3LB); (d) Flying Capacitor (FC) (e) Neutral-point-clamped (NPC) and (f) T-Type (TT). Main unidirectional topologies employed to implement the hybrid and/or passive cells of the MTB DC-DC converter: (g) (a) Semi-active bridge rectifier (SABR); (h) Full-wave rectifier (FWR) and (i) Voltage-doubler rectifier (VDR).

stages can be implemented by using different active, semi-active (hybrid), and passive topologies [47], like those shown in Figure 10, and also by the association of devices in parallel.

Thus, based on the relation between the blocking voltage V_{DS} and the on-state resistance for MOSFETs ($R_{DS(ON)} \propto V_{DS}$) [44], [46], [48], the MTB topologies, in particular the asymmetrical ones, can be comparatively evaluated in terms of the $R_{DS(ON)}$ for a specific material and semiconductor chip area A_{SE} [cf. (8)], which is denoted as specific on-resistance [$\Omega \text{ cm}^2$].

$$R_{DS(ON)} \cdot A_{SE} \approx \left[\frac{k_{SE} V_{DC, total}}{k_{sw} N_{cell, i, j} (N_L - 1)} \right]^{2.5} \quad (8)$$

Where $N_{cell, i, j}$ is the number of cells in one side of the MWT; N_L is number of voltage levels of the active bridge [cf. Figure 10 (a)-(f)]; $V_{DC, total}$ is the total voltage across the MTB DC-DC converter terminals; k_{sw} is the voltage utilization factor of 60% (i.e. $k_{sw} = 0.6$), which defines a safety margin, considering the maximum blocking voltage and possible overvoltages on the device. k_{SE} is related to the material and structure of the semiconductor, such as Si, SiC or Gallium-Nitride (GaN) [44], [48].

From (8), it is noticed that the semiconductor losses of the N_L -Level cells can be reduced and distributed over sev-

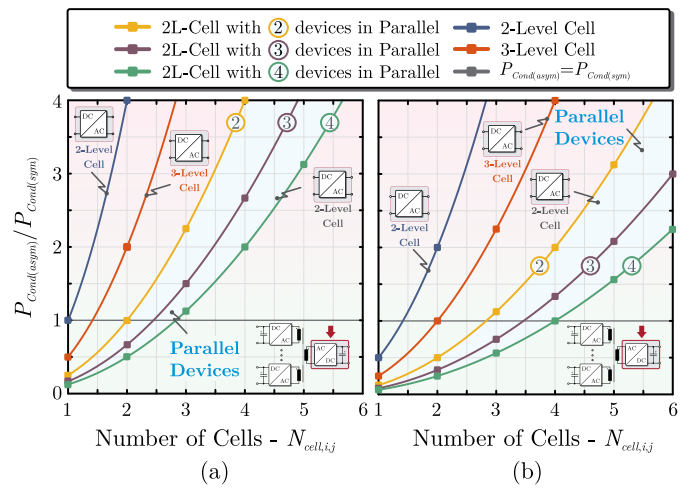


Figure 11. Relation between the conduction losses for the both configuration, considering only 2-Level cells on the SMTB DC-DC converter ($N_{L, sym} = 2$) and different combinations on the ASMTB one employing: (a) the same devices (i.e. $k_{ron} = 1$) and (b) devices in the insulation cell with half of the $R_{DS(on)}$ adopted to symmetrical one (i.e. $k_{ron} = 0.5$). The different combinations on the asymmetrical configuration include the 3-Level and 2-Level cells with one and multiple devices in parallel.

eral devices. As a result, this leads to a slight increment in the junction temperature (T_j) and allows for selecting smaller semiconductor chip area (A_{SE}) or for maintaining high-efficiency and high-reliability. Furthermore, in order to assess the power losses on the MTB converters, the active bridges aforementioned (cf. Figure 10) are combined into both architectures: SMTB and AMTB topologies (cf. Figure 3). Thus, assuming that the switching losses P_{Sw} are neglected ($P_{Sw} \approx 0$), once the converters present soft-switching (ZVS and ZCS), and they process equal power at the same voltage, the relation between the conduction losses P_{Cond} for AMTB and SMTB topologies are expressed by (9) and depicted in Figure 11 (given that $P_{Cond} \propto R_{DS(on)} \propto I_{rms}^2$).

$$\frac{P_{Cond, AMTB}}{P_{Cond, SMTB}} = k_{Ron} N_{cells, i, j}^2 \left(\frac{N_{L, sym} - 1}{N_{L, asym} - 1} \right) \quad (9)$$

Whereas, k_{Ron} is a scaling factor associated to the semiconductor technology used to compose the insulated cell of the AMTB topologies. When $k_{Ron} = 1$, the power devices employed in both configurations are equal. However, when k_{ron} is monotonically reduced, the performance of the adopted power device is significantly improved (e.g. wide-band gap device with lower $R_{DS(on)}$), so that $0 < k_{Ron} \leq 1$. Thus, as shown in Figure 11 (b), devices with lower $R_{DS(on)}$ can reduce the conduction losses and improve the performance of the AMTB topology. Therefore, an optimized design can be carried out to find the optimum architecture, number of cells, and power device, as presented in [17], [18]. Finally, hybrid/passive topologies can also be used to implement the cells for reducing the volume trough the elimination of inherent auxiliary circuits, cf. Figure 10 (g)-(i) [26].

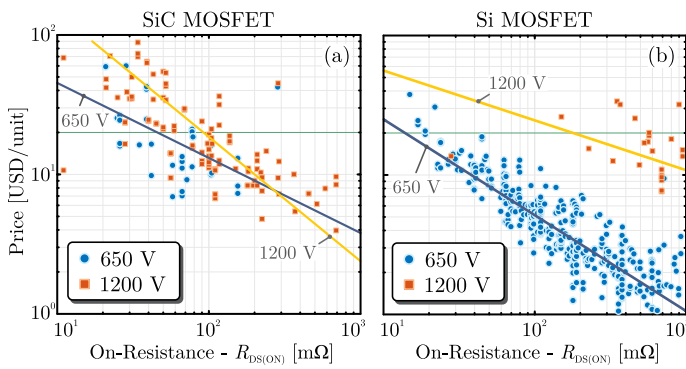


Figure 12. Relation between the price (per unit) of the power semiconductor device and the on-resistance for a blocking voltage of 650 V and 1200 V: (a) Silicon Carbide (SiC) and (b) Silicon (Si) MOSFETs. The prices were extracted from the main sellers, considering the active parts of all packages and manufacturers. The straight lines represent the fitting function of the data.

D. Cost-Benefit

Thanks to the core material (cf. Figure 5) and number of cells reduction, the MTB topologies, in particular those based on the asymmetrical configuration might be more advantageous in terms of cost compared to the solution based on multiple converters employing 2WT. Thus, with a reduction of the number of cells, the cost-benefit can also be extended to the power semiconductor devices. In a first analysis, the devices used to compose the symmetrical architecture can be all associated in parallel at the insulated cell [cf. Figure 3 (b)] for processing the same power (i.e. $P_{DC,asym} = P_{DC,sym}$). Therefore, it is clear that the reduced number of printed-circuit boards and auxiliary circuits will lead to a cost-benefit. However, to avoid parallelism of several switches in AMTB topologies, power semiconductor devices with lower $R_{DS(ON)}$ are required to ensure nearly the same efficiency compared to the symmetrical one. Thus, a scaling law relating the on-resistance with the number of cells can be used to define the required $R_{DS(ON)}$ value for an asymmetrical architectures [cf. (10)] and then its total costs.

$$R_{DS(ON),asym} \leq (N_{cells,pri})^{-1} \cdot R_{DS(ON),sym} \quad (10)$$

Where, $R_{DS(ON),asym}$ and $R_{DS(ON),sym}$ are the required on-resistance of the AMTB and SMTB topologies, respectively. This scaling law considers that the conduction losses are proportional to the power processed by the cells and also on-resistance value (i.e. $P_{Cond} \propto P_{DC} \propto R_{DS(on)}$).

As a matter of comparison, the estimated cost of the MTB topologies considering the power semiconductor devices can be defined in terms of the number of cells employed in both the SMTB and AMTB DC-DC converters, as expressed by (11) and (12), respectively. Where (C_{SMTB}) and (C_{AMTB}) are the estimated cost of both MTB topologies, N_{MOS} is the number of devices in each cell [cf. Figure 10], and σ_{MOS} is the cost of a single power semiconductor device.

$$C_{SMTB} = \sigma_{MOS,sym}(2N_{cell,pri}N_{MOS}) \quad (11)$$

$$C_{AMTB} = \sigma_{MOS,sym}N_{MOS} \left(N_{cell,pri} + \frac{\sigma_{MOS,asym}}{\sigma_{MOS,sym}} \right) \quad (12)$$

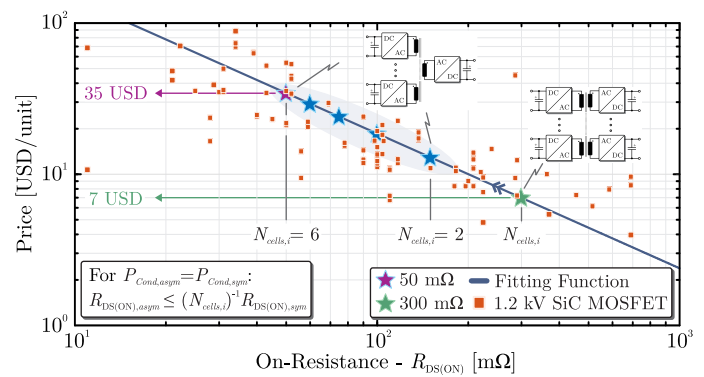


Figure 13. Unit Price of the power semiconductor device in function of the on-resistance ($R_{DS(ON)}$) and number of cells ($N_{cells,pri}$) considering 1.2 kV SiC MOSFETs in asymmetrical and symmetrical architecture. The analysis is performed considering a device with an on-resistance equal to 300 mΩ for the symmetrical architecture, as reference (i.e. $R_{DS(ON),sym} = 300$ mΩ).

In both cases, the cells are considered identical (i.e. the same number of devices per cell) with the exception of the insulated cell in the AMTB topologies that can present different power semiconductor device to handle the higher current. Thus, the cost-benefit will be only obtained by the AMTB topologies whether the price of a single power device $\sigma_{MOS,asym}$ respects the condition (13).

$$\frac{\sigma_{MOS,asym}}{\sigma_{MOS,sym}} \leq N_{cell,pri} \quad (13)$$

From the unit price of the MOSFETs in dependency of on-resistance [cf. Figure 12 (a) and (b)], and by using its fitting function, the cost analysis among the both architecture is estimated for 1.2 kV SiC as a function of the number of cells (cf. Figure 13). Thus, in order to summarize the previous analysis, Table III presents the total cost analysis between the SMTB and AMTB converters, taking into account the unit prices from Figure 13 for different number of cells. In this analysis was considered that the cells are implemented by using the same active bridge FB (cf. Figure 10), which has four devices per cell, i.e. $N_{MOS} = 4$.

As can be seen, although higher current rating devices (with lower on-resistance) are required to implement the insulated cell of the AMTB topologies, the increased price of the individual device does not impact further the total cost. On the contrary, even with the lower $R_{DS(ON)}$, it is possible to reduce around 15% of the power semiconductor costs. Therefore, depending on the design constraints and requirements, power semiconductor devices with lower $R_{DS(ON)}$ can afford certain cost-benefit in AMTB topologies, cf. [16], [18].

In this context, the higher current also affects the thickness of the cooper wires of MWT, enlarging its cross-section area. However, the cooper cost to build either symmetrical MWT (even multiples 2WT) or an asymmetrical MWT can be assumed equal at the same power level. In other words, the thick cooper wire used in the asymmetrical MWT can be considered as the union of the all individual windings in only one, cf. Figure 5 (c). Apart of that, it should be noted that the cooper cost (C_{Cu}) is proportional to power processed by the winding ($S_w = v_{rms}i_{rms}$). Thus, considering the same

Table III
TOTAL COST ANALYSIS BETWEEN THE SMTB AND AMTB TOPOLOGIES CONSIDERING THE DATA FROM FIGURE 13 AND $N_{MOS} = 4$.

$N_{cells,pri}$	2 cells	3 cells	4 cells	5 cells	6 cells
Maximum $R_{DS(ON),sym}$	300.0 mΩ	300.0 mΩ	300.0 mΩ	300.0 mΩ	300.0 mΩ
Selected Devices - SMTB Topology	IMW120R220M1 - 288.0 mΩ and $\sigma_{MOS,sym} = 7$ USD				
Total Cost C_{SMTB}	109 USD	168 USD	224 USD	280 USD	336 USD
Selected Devices - Primary-Side Cells	IMW120R220M1 - 288.0 mΩ and $\sigma_{MOS,pri} = 7$ USD				
Maximum $R_{DS(ON),asym}$	143.0 mΩ	95.3 mΩ	71.5 mΩ	57.2 mΩ	47.6 mΩ
Selected Devices - Insulated Cell	IMW120R090M1 110 mΩ	C3M0075120D1 75 mΩ	NTH4L040N120SC1 58 mΩ	IMW120R030M1 40 mΩ	C3M0021120D 28 mΩ
Unit Price - $\sigma_{MOS,asym}$	9 USD	12 USD	14 USD	20 USD	35 USD
Total Cost - C_{AMTB}	93 USD	132 USD	168 USD	220 USD	308 USD
Cost Reduction	15.60 %	21.43 %	25.00 %	21.43 %	8.33 %

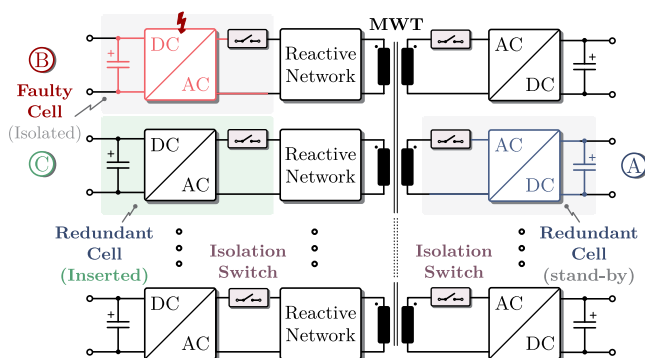


Figure 14. Generic scheme of the proposed fault-tolerant based on multi-winding redundancy approach: (A) normal operation with redundant cells in stand-by mode and others in power-sharing mode (as part of the MTB DC-DC converter), (B) reconfiguration example after a fault by means of the isolation switches to disconnect the faulty cell and (C) connect the redundant cell previously in stand-by (or just routing the power by the healthy ones).

voltage on the windings, the cost becomes proportional to the current which flows through the winding, i.e. $C_{Cu} \propto S_w$ [18].

E. Multiwinding Fault-tolerant Capability

Another advantage and potential of the MWT is related to the redundant power path, which provides fault-tolerant capability by means of the magnetic coupling among the cells. As the cells are connected to the same core, in case of a fault, the faulty cell can be isolated from the converter and then the power flow can be routed among the healthy cells. Accordingly, the operation is kept without affecting the availability and the maintenance costs due to some interruption of the operation.

The proposed fault-tolerant approach aims at the realization of a topology with particular attention to the continuous operation of the system, even under faulty conditions. For that reason, the fault-tolerant scheme is composed by isolation switches (i.e. bidirectional arrangement of power semiconductors), which acts directly on the cells, disconnecting them in case of fault. Similarly, the same switches can be used to reconnect the cell in order to restore the thorough operation.

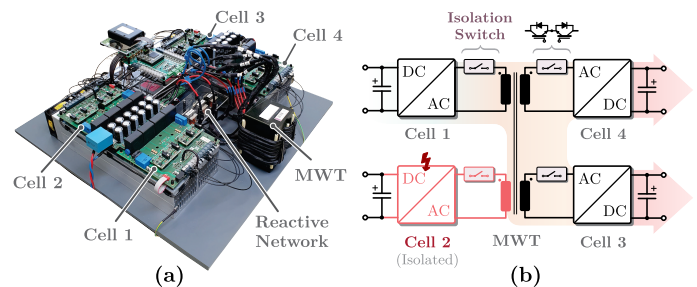


Figure 15. (a) Hardware prototype of the SQAB converter. (b) Power flow on the SQAB considering a fault at the cell 2.

In Figure 14, the main cells of the power converter are at the same time the redundant parts that are operating in power-sharing mode. In normal conditions, all cells of the converter operate simultaneously, sharing the power among the cells. In case of a fault, only the faulty cell is isolated from the entire system [cf Figure 14], whereas the healthy cells maintain the power flow and the system operating. Moreover, the converter can also be designed considering extra windings, so that stand-by cell might be integrated to the system. Both approaches are equally feasible, the implementation will depend only on the design requirements and constraints from each application.

In order to verify the performance of the proposed fault-tolerant approach based on the MWT, a prototype of a symmetrical QAB (SQAB) converter was built and experimental results were obtained, cf. Figure 15 (a). The converter operates in open-loop and the gating signals are generated by the digital signal processor (DSP). To evaluate dynamically the performance of the converter under fault case [cf. Figure 15 (b)], a short-circuit on the cell 2 was emulated by software in the DSP (TMS320F28379D), as investigated in [49].

Figure 16 presents the main waveforms of the SQAB converter operating dynamically before and after a fault at the cell 2 (cf. Figure 16). The dynamic behavior during the fault at the cell 2 is depicted in Figure 16 (a), demonstrating that the converter maintains operational after the failure and the immediate disconnection of the faulty cell (through the isolation-switch), cf. Figure 16 (b). As can be observed, while

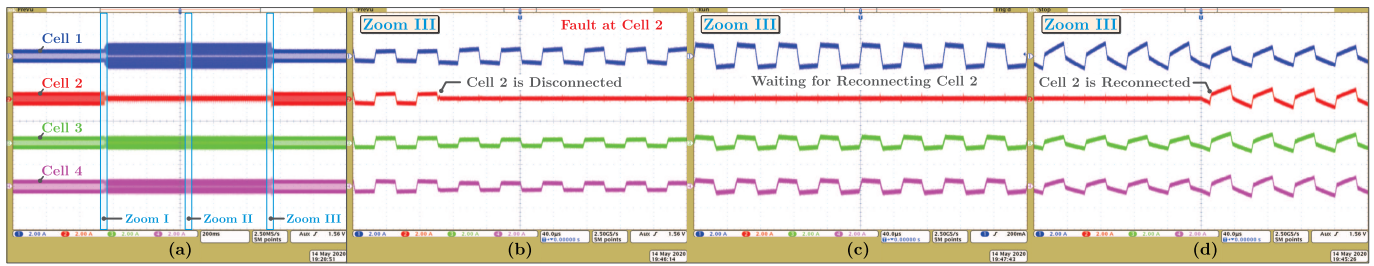


Figure 16. Experimental results of the SQAB: (a) dynamic behavior of the SQAB converter before, during and after the fault; (b) highlighting the disconnection of the cell 2 when the fault is detected; (c) partial operation after the disconnection of the cell 2; and (d) when the cell 2 is reinserted to the system and the total power flow is restored.

the cell 2 is not reconnected to the system, cell 1 processes more power to compensate the absence of cell 2, keeping the partial power flow (nearly the rated power), cf. Figure 16 (c). After the fault, the system verifies if the fault was cleared and then if the isolated-cell remains healthy to be reconnected to the converter, cf. Figure 16 (d). Otherwise, it is reconfigured to partial load mode: the faulty cell remains disconnected and the power flow is adjusted for the resulting topology (i.e. TAB).

F. Reliability and Availability Assessment

As the MTB topologies are composed of several cells, the total number of employed components is increased compared to an equivalent single converter system. In effect, this increases the probability of a failure of a component or cell [50]–[53]). However, in contrast to the single converter system, the failure of a single component does not necessarily conduct to a failure of the whole converter, since only one cell is affected. As previously shown, depending on the architecture of the converter and the failure, it can still be functional in partial power flow. Thus, minimizing the failure of those elements and mainly their impact, the overall reliability (R_{sys}) and availability (A_{sys}) can be enhanced, cf. (14) and (15).

$$R_{sys}(t) = R_{sys}(0) \cdot e^{-\int_0^t \lambda_{sys}(\tau) d\tau} \quad (14)$$

In (14), $R_{sys}(t)$ is the reliability function; $R_{sys}(0)$ is the initial reliability of the system, i.e. when $R_{sys}(0) = 1$, the system is fully functional at initial state; $\lambda_{sys}(t)$ is the failure rate, which indicates the number of failures per unit time (i.e. one failure in the time: 1 FIT = 10^{-9} failure/hour).

$$A_{sys} = \frac{MTTF}{MTTF + MTTR} \quad (15)$$

Whereas in (15), MTTF is the expected time before a failure occurs and MTTR is the mean repair time that it takes to eliminate a failure and to restore the system operation. The repair time depends on maintainability, such as effective diagnosis of faults, operational time to replace the faulty cell and so on. In contrast to reliability, MTTF provides only the average time that the system operates without failing. The relation between MTTF and $R_{sys}(t)$ is defined by (16), when $\lambda_{sys}(t)$ is constant (i.e. $\lambda_{sys}(t) = \lambda_{sys}$) [54]–[56].

$$MTTF_{sys} = \int_0^{+\infty} R_{sys}(\tau) d\tau = \frac{1}{\lambda_{sys}} \quad (16)$$

Since the failure rates of the reactive network along with MWT are much lower than those of semiconductors and DC-Link capacitors, their failures are neglected [53], and any fault in the capacitors and semiconductors might lead the cell to fail. As a matter of fact, it is assumed that the system is non-repairable, and it is capable of fault detection, isolation, and reconfiguration, i.e., the system has an effective fault management [49]. Moreover, considering that the all cells are equal and the failure rate of each cell λ_{cell} are constants, the mean time to failure ($MTTF_{sys}$) for the entire system with N_{cells} in symmetrical and asymmetrical configuration (cf. Figure 3) can be estimated by (17) and (18), respectively.

$$MTTF_{sys,sym} = \frac{1}{2N_{cells}\lambda_{cell}} \quad (17)$$

$$MTTF_{sys,asym} = \frac{1}{(N_{cells} + k_{fail})\lambda_{cell}} \quad (18)$$

In that case, λ_{cell} is defined by: $\lambda_{cell} = \lambda_{Cap} + \lambda_{Sw}$, so that $\lambda_{Cap} = (\sum_k \lambda_{Cap,k})$ and $\lambda_{Sw} = (\sum_k \lambda_{Sw,k})$ are the failure of the all capacitors and power devices employed in the cell, respectively; and k_{fail} is the failure factor, which indicated the relation between λ_{cell} from the symmetrical configuration with failure ratio of the insulated cell λ_{icell} from the AMTB topologies, so that $k_{fail} = (\lambda_{icell}/\lambda_{cell}) \geq 1$. In other words, due to the fact the total power in an AMTB converter is merged and processed by only this insulated cell, the current efforts are higher and thus its failure rate might also be higher ($\lambda_{icell} \geq \lambda_{cell}$), i.e. $\lambda_{icell} \propto k_{fail} \propto N_f$, according to (19).

$$N_f = k_1(\Delta T_j)^{k_2} \cdot \left[e^{-k_3(T_{j,av} + 273^\circ\text{C})} \right] \quad (19)$$

Whereas N_f is the number of thermal cycles to failure; ΔT_j is the magnitude of the thermal variation; $T_{j,av}$ is the average junction temperature during this variation; and k_1 , k_2 , and k_3 are fitting parameters [48], [52], [57], [58].

Comparatively, from a system-level perspective, the MTTF of a system composed by multiple 2WT-based converters ($MTTF_{sys,2WT}$) can be easily obtained from (17). In that case, even when only one single cell fails, in fact, two cells are removed of the power flow, since the multiples DC-DC converter based on 2WT are not coupled magnetically among them. Hence, $MTTF_{sys,2WT} = (MTTF_{sys,sym}/2)$, as expressed in (20) and illustrated in Figure 17.

$$MTTF_{sys,2WT} = \frac{1}{2N_{cells}\lambda_{cell,2WT}} = \frac{1}{4N_{cells}\lambda_{cell}} \quad (20)$$

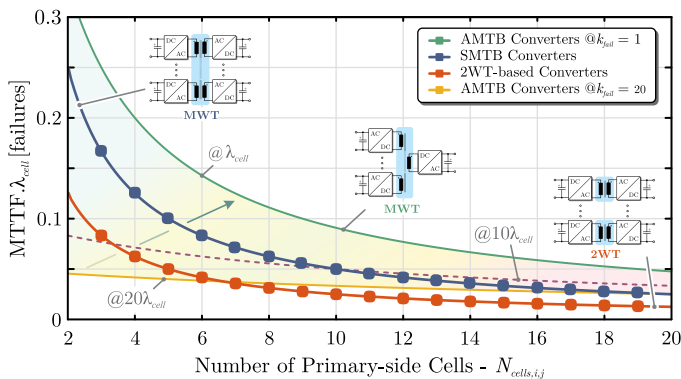


Figure 17. Failure behavior of the asymmetrical and symmetrical configuration based on the MWT and 2WT, considering the number of cells employed in each architecture and also the different failure rates of the insulated cell.

As can be seen, for $\lambda_{icell} = \lambda_{cell}$, the asymmetrical configuration exhibits a higher MTTF compared to the symmetrical configuration using MWT and 2WT, due to the reduced number of components. However, as long as λ_{icell} rises toward to an elevated failure rate in order to access fairly the MTB topologies (e.g. $k_{fail} = 20$ and hence $\lambda_{icell} = 20\lambda_{cell}$), the $MTTF_{syst,asym}$ reduces in accordance with (18). However, even for failure rate ten times higher ($k_{fail} = 10$), which is quite significant, the asymmetrical configuration still shows some advantage. Therefore, based on the MTTF, the overall AMTB topologies might have superior performance compared to the other two architectures, providing an elevated lifetime before some failure.

Nevertheless, the MTTF neglects the consequences on the operation whether a fault occurs at the insulated cell. In that case, a failure in this cell can interrupt abruptly the power flow, since it is completely merged in a single power path through the insulated winding of the MWT (secondary side, cf. Figure 3). As a result, even with a considerable MTTF, the particular case where the AMTB topology is composed of only an insulated cell can experience a blackout, reducing the availability by increasing the mean time to repair (i.e. MTTR). In this scenario, one possible solution to ensure the availability, and thus the continuous operation of the AMTB topologies, is performed by adding stand-by redundant cells along with the insulated cell, so that (18) can be rewritten as (21).

$$MTTF_{syst,asym} = \frac{1 + N_{red,stab}}{(N_{cells} + k_{fail})\lambda_{cell}} \quad (21)$$

The addition of $N_{red,stab}$ stand-by redundant cells allows to achieve a redundancy, where the system is operational as long as N_{cells} cells are functional out of total cells (i.e. $N_{cells} + N_{red,stab}$). Although the initial cost to insert these redundant cells is a part of the whole system (depending on the total number of cells), this cost tends to become high over time, since the cells are not providing any service to the system. Therefore, from the continuous operation point of view, the architecture considering at least two cells is recommended ($N_{cells,i,j} \geq 2$), once the MWT fault-tolerant capability can be used to overcome possible interruptions and to mitigate the maintenance efforts.

G. Challenges of MWT in MTB Topologies

The advantages of the common magnetic core come at the expense of specific challenges related to the operation of MTB Topologies (cf. Figure 18). The majority of MWT topologies are based on non-resonant operation mode. Although resonant converters are known for their advantageous characteristics like high-efficiency and soft-switching operation across a wide load range, only a few works have been done on the topic of resonant MTB topologies. In particular, the predominant reason is the complex frequency modulation of the coupled ports. Furthermore, limiting factors arise from the practical requirement for splitting the resonant tank on the different reactive networks. In most publications the resonant tank elements are located in the reactive network of each module in order to allow equal conditions for bidirectional power flow [37] [42]. Moreover, due to the complex transfer functions, the desired power sharing of the ports is challenging. In [38], it was shown that the power sharing between the ports can be achieved with a specific ratio of resonant inductances. However, the MTB topologies based on LLC converter are designed with equal resonance frequency and operate with a fixed frequency and duty cycle. Therefore, the only degree of freedom to adjust the power flow of each cell is made by the DC input voltages, which requires another conversion stage for the DC voltage adaptation, as presented in [38].

Moreover, the higher complexity in the transformer design makes the MWT topologies more susceptible to deviations of the stray elements of the MWT. Deviations in the stray elements can lead to unequal power transfers among the cells. The issue of unwanted couplings between load ports can occur due to load changes in one output port. Although the cells are isolated from each other, through the common magnetic core, the load change of one port will affect the other cells. In particular, the effects of parameter deviations and unwanted couplings depend heavily on the configuration of how the cells are interconnected. Thus, the next section provides an overview about different interconnections, the resulting effects of the MWT issues related to different interconnection possibilities and measures how to mitigate these effects.

IV. INTERCONNECTION AND OPERATION MODES ISSUES IN MTB DC-DC CONVERTERS

1) *Module Interconnection:* With respect to the interconnection between the terminal ports, the cells can be interconnected in one of the configurations listed in Table IV (cf. Figure 19) [46], [59]. As can be seen, there are basically three possible connections: series, parallel and independent;

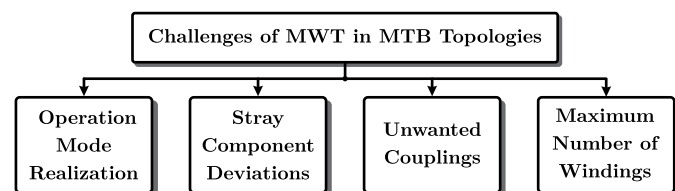


Figure 18. Main challenges of MWT in MTB topologies.

Table IV
CLASSIFICATION OF THE MULTI-WINDING CONVERTER ASSUMING A POWER FLOW FROM PRIMARY (INPUT) TO SECONDARY SIDE (OUTPUT).

Ports	ISOS	ISOP	IPOS	IPOP	IIOI	IIOS	ISOI	IIOI	IPOI
Input [I]	Series	Series	Parallel	Parallel	Independent	Independent	Series	Independent	Parallel
Output [O]	Series	Parallel	Series	Parallel	Independent	Series	Independent	Parallel	Independent

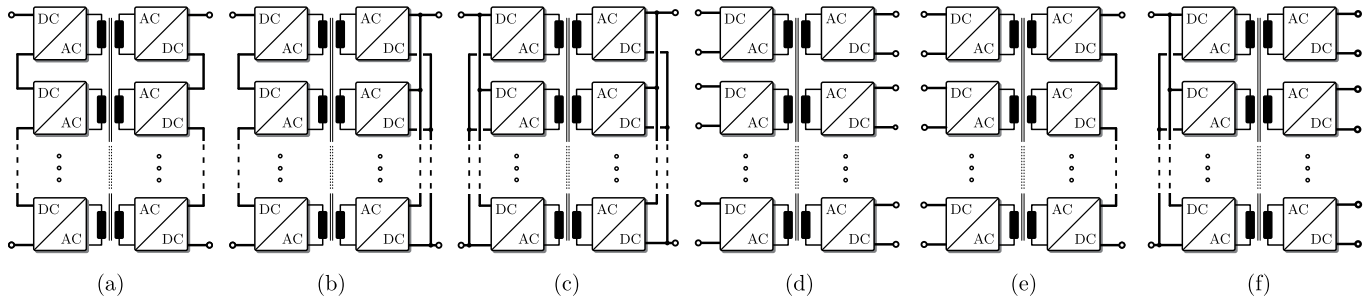


Figure 19. Possible configurations used to interconnect the modules in the MTB topology: (a) input-series output-series (ISOS); (b) input-series output-parallel (ISOP) or input-parallel output-series (IPOS); (c) input-parallel output-parallel (IPOP); (d) input-independent output-independent (IIOI); (e) input-independent output-series (IIOS) or input-series output-independent (ISOI); input-independent output-parallel (IIOI) and input-parallel output-independent (IPOI).

which can be mixed among them in order to reach the properly configuration depending on the application requirement. Moreover, these different interconnections allow to either share the current between the converter modules with parallel interconnection or distribute the voltage between the converter cells with series interconnection. For the case of isolated sources or loads, the cells are kept separated, so that each cell is connected directly to one of these isolated sources or loads. Therefore, regardless the architecture configuration and symmetry, the cells can have different voltage/current levels and at same time they can share power among them independently from the others. It means that the MTB topologies can have several configurations, making its applicability extremely wide and suitable for all power, voltage and current levels.

A. Deviations in the Stray Components of the MWT

The increased number of windings might lead to a more complex MWT design. Thereby, one important parameter is the leakage inductance of each winding which contributes to the inductance of the reactive network. Depending on the arrangement of the windings, the value of the leakage inductance in each winding might differ. In MAB converters [cf. Figure 20 (a)], this inductance is a key parameter which defines the power transfer of the related port. A port with a smaller inductance will transfer more power compared to a port with a higher one [cf. Figure 20 (b)-(c) and (f)-(g)]. Thus, depending on the module interconnection, an unequal and undesirable power flow is created among the cells.

In particular, the independent connection will lead to large deviations on the current due to the resulting output-voltage imbalance, cf. Figure 20 (g). Thus, in order to balance the power flow, the phase-shifts among the ports have to be adapted. However, this might lead to higher circulating currents. Therefore, to avoid the unequal power transfer characteristic, without adapting the phase-shift, is used different extra inductances in the reactive network. Hence, the total inductance in the reactive network can be equalized in each port.

For the resonant operation mode, deviations in the reactive network will lead to different characteristics of the resonant tank and hence to different power transfer characteristics, cf. Figure 20 (d)-(e) and (h)-(i). Thus, the parameters in the resonant tank need to be adjusted in order to balance the power flow, so that these issues show the importance of the MWT design for the MTB converters. Especially the avoidance of deviations in the leakage inductance of the individual windings is of particular importance.

B. Unwanted cross-coupling Effects

The issue of unwanted cross-coupling effects describes the interaction between load ports due to the magnetic coupling. In other words, when the output characteristic of one port is changed, the other ports will also be affected [25]. This effect is severe for architectures with independent load ports (ISOI, IPOI, IIOI), especially for operation modes with large difference in power/voltage level.

For instance, in a MAB topology a load step in one of the load ports will require an increase in phase-shift of the related output port. However, due to the magnetic coupling, the power transfer of the other load ports will be affected and a readjusting of their phase-shifts is required. As a result, the readjusting of the phase-shifts leads to a relative phase-shift and hence to higher circulating currents in the converter.

In literature, the problem of cross-coupling in MAB converters is mainly addressed with strategies which allows individual control of the load ports [27] [60]. In general, the existing control concepts for MTB converters pursue the target to simplify the control structure to multiple independent control loops with single input single output characteristic, like in conventional 2WT-based converter. However, the physical effects of the cross-coupling are still present so that the circulating power is not fully eliminated. Another way to decouple the output ports can be realized with a specific inductance ratio between the feeding ($L_{Feed,i}$) and the sinking ports ($L_{Sink,j}$) [28].

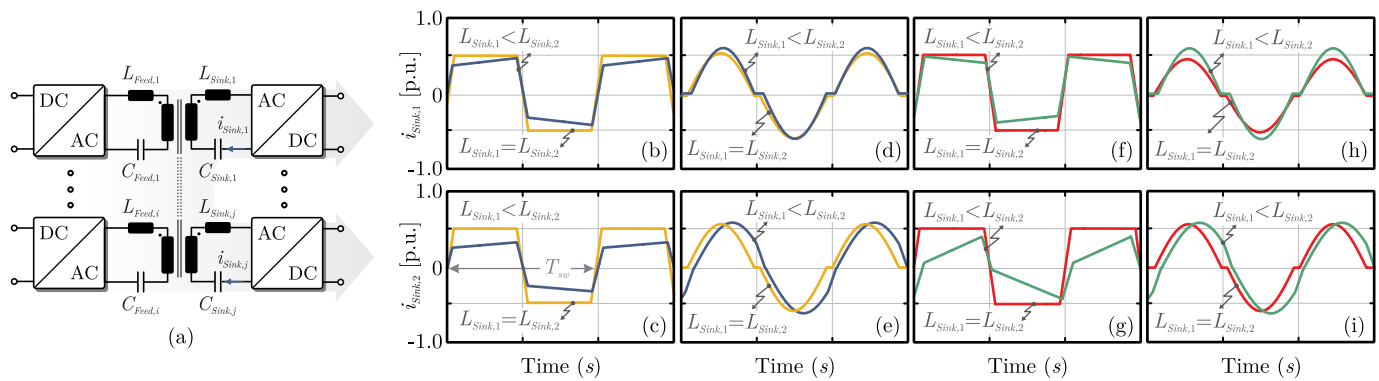


Figure 20. Effects of parameter variations in the reactive network of the (a) MTB DC-DC converter considering: (b)-(c) parallel interconnection in non-resonant mode; (d)-(e) parallel interconnection in resonant mode. Similarly, considering (f)-(g) independent interconnection in non-resonant mode and (h)-(i) independent interconnection in resonant mode.

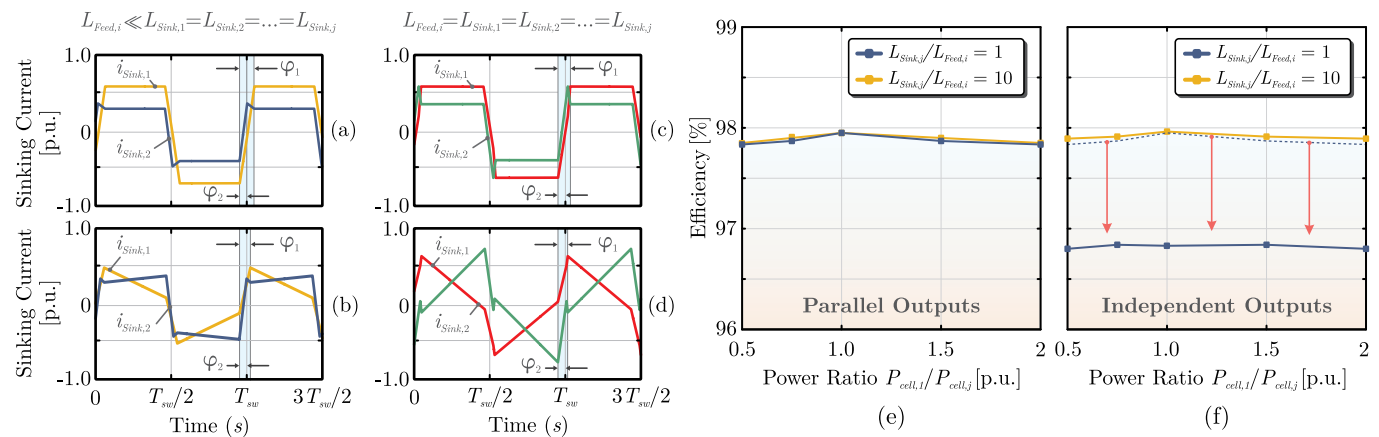


Figure 21. Effects of cross-couplings due to a load variation in one output port in dependency of the output configuration for different inductance ratio ($L_{Sink,j}/L_{Feed,i}$): (a) Parallel output configuration; (b) Independent output configuration; (c) Load ports transformer currents for parallel output configuration; (d) Load ports transformer currents for independent output configuration. Whereas (a)-(b) are decoupled and (c)-(d) are not decoupled.

Figure 21 shows the relation between the choice of the reactive network inductance and the decoupling of the output ports. In this scenario, the power of one load port is increased two times the power of the other output ports.

Further, for the independent load case, the related output voltage $V_{DC,1}$ is assumed to be higher. Figure 21 (a)-(c) show the system with a common DC-link at the output ports (i.e. parallel interconnection). The choice of the inductance ratio only influences slightly the current waveforms. For independent load ports, the choice of the inductance ratio significantly affects the coupling [cf. Figure 21 (b),(d)]. The resulting distortion in the current and the higher peak currents deteriorates the efficiency for cases with a low ratio of ($L_{Sink,j}/L_{Feed,i}$) which results in a strongly coupled system [cf. Figure 21 (f)]. Whereas, for configurations with a common DC-link at the output (parallel configuration), the degree of decoupling has only limited influence on the converter efficiency [cf. Figure 21 (e)].

The influence of the inductance ratio on the cross-coupling for independent load ports has been experimentally validated (cf. Figure 22) in a TAB converter, considering two load ports. Thus, for an inductance ratio of ($L_{Sink,j}/L_{Feed,i}$) = 1, the output voltage is changed by 10% of the rated voltage

on port 2. This leads to a large change in the transformer current ($i_{Sink,1}$) of the unchanged load port 1, increasing the current effort on the devices. For the decoupled ports with an inductance ratio of ($L_{Sink,j}/L_{Feed,i}$) = 5, a load change at port 2 does not impact on the power transfer characteristic of port 1. The current $i_{Sink,1}$ of the unchanged port stays nearly constant after the voltage-step in port 2. To achieve the desired inductance ratio, extra inductances can be placed in the load ports. However, increasing this inductance in a MAB configuration might lead to higher circulating current [17]. Thus, there is a trade-off between the decoupled ports and total inductance, which can be achieved by some winding arrangements.

C. Maximum Number of Windings in a MWT

Further, the size constraints of the MWT needs to be considered. The larger the number of windings, the larger will be the required window area of the magnetic core. Thus, the maximum available number of windings is limited by the commercial off-the-shelf available magnetic cores, as illustrated in Figure 23. Theoretically, custom made larger magnetic cores could be used but this option is not considered, due to the higher expected costs. The resulting requirements

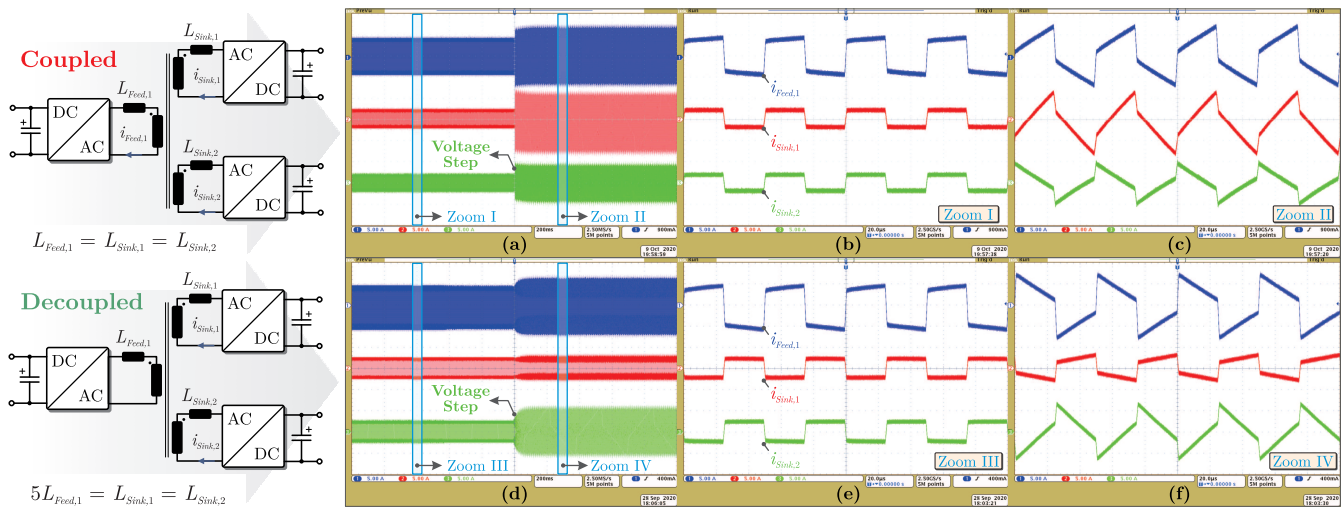


Figure 22. Effects of cross-couplings in TAB converter (cf. Figure 20 (a)) with one feeding-port and two sinking-ports, considering independent interconnection among the ports for different inductance ratio ($L_{Sink,j}/L_{Feed,i}$): (a)-(c) current on the MTW when the cells are coupled; whereas (d)-(f) they are decoupled.

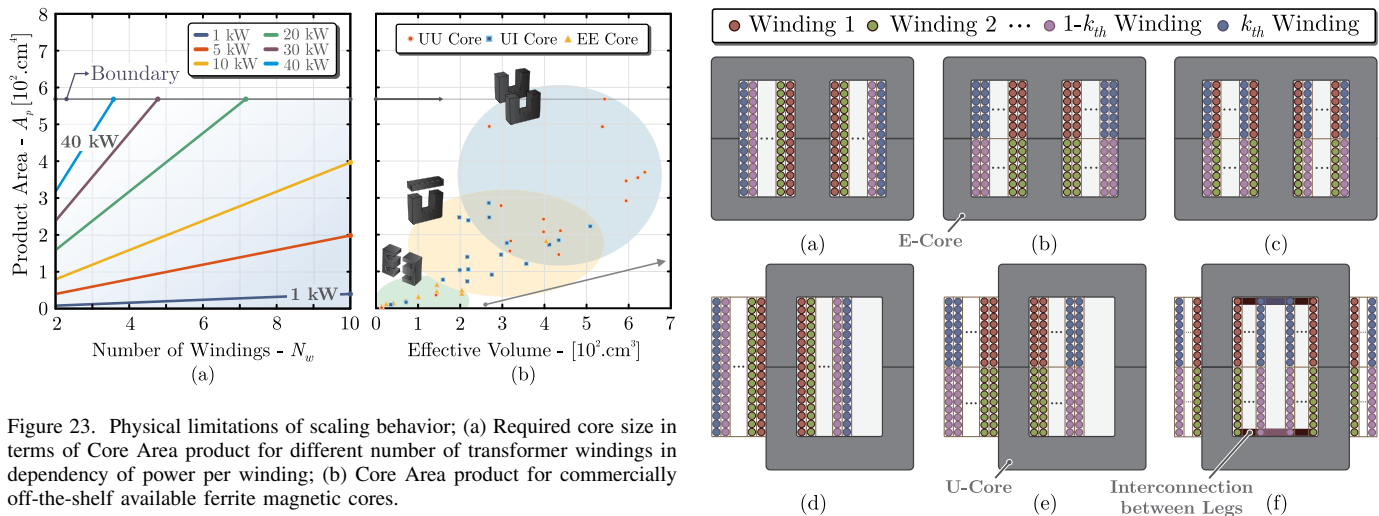


Figure 23. Physical limitations of scaling behavior; (a) Required core size in terms of Core Area product for different number of transformer windings in dependency of power per winding; (b) Core Area product for commercially off-the-shelf available ferrite magnetic cores.

regarding the magnetic core size with respect to the number of windings is evaluated with the area product A_p , whose formula has been derived in (1) for a MWT. The required area product is compared with available cores from different manufacturers.

Thus, Figure 23 summarizes the limitations in terms of maximum number of windings with respect to different power levels per winding. Considering the largest available core core U126/91/20 (UU cores) from magnetics with the product area ($A_p = 572 \text{ cm}^4$), the power processed by the MWT is limited to $P_{MWT} = 143 \text{ kW}$, so that the power can be divided among the windings. For configurations with less number of windings and lower power, the usage of E-cores (e.g. planar cores) can be a good option [61]. Yet, it should be noted that theoretically the window area of the core can be increased further by inserting an I-core between the two outer cores (i.e. UIIU).

D. Typical Winding Arrangement of MWT

The previous considerations revealed the importance of a proper winding arrangement in MWT. Depending on the application field and the module interconnection, the optimum

Figure 24. Possible winding structures for MWT considering E-cores: (a) Layered structure; (b) Stacked structure; and (c) Interleaved stacked structure. Considering U-cores: (d) Layered structure; (e) Stacked structure; and (f) Interconnected-leg stacked structure.

winding structure might differ. In general, existing winding structures for conventional 2WT can be extended to MWT, which is shown for a k th winding transformer in shell-type and core-type winding arrangement (cf. Figure 24). However, some winding structures might not be beneficial to be used in MWT. For instance, a layered (concentric) winding structure [cf. Figure 24 (a) and (d)], leads to large unbalances in the leakage inductances of the ports due to the different distances between the windings. Furthermore, stacked (also referred to sectioned [17]) winding structures depict another solution, cf. Figure 24 (b) and (e), for EE and UU configuration, respectively. On the other hand, interleaved stacked winding structures further improve the coupling among the windings, cf. Figure 24 (c). As an additional winding arrangement for core-type MWT, the interconnected-leg stacked structure arise to further reduce deviations in the leakage inductance

by interchanging the windings between the legs of the UU configuration, cf. Figure 24 (f). Thus, these basic structures can be combined in order to achieve the desired transfer characteristic with respect to different module interconnection configurations, as shown in Figure 19. For example an ISOI module interconnection with individual load ports requires a high impedance between the load ports in order to limit the undesired cross-coupling effects. At the same time the coupling between the feeding- and sinking ports should be as high as possible. Therefore interleaved stacked winding structures might be more advantageous.

V. QUANTITATIVE ANALYSIS OF THE MTB DC-DC CONVERTERS

Different configurations of the MTB DC-DC converters and some of their possible topologies based on DAB, SR and LLC were presented in Section II. In order to verify quantitatively the converters performance in terms of efficiency, losses and power density, some topologies were simulated using the MATLAB/Simulink and the PLECS toolbox, considering the electrical specifications described in Table V and also the

parameters presented in Table VI. For the MWT, it was assumed the same magnetic core (E80/38/20) and the same wires on the primary-side windings for all topologies. The difference of the MWT among the evaluated MTB topologies remains on the winding arrangements and on the wires of the insulated winding, which is obtained by the association of all secondary-side wires in parallel, as discussed in Section III.

In total, there are nine converters, where three of them are non-resonant and the other six are resonant, as listed in Table VII. Among the non-resonant, it was evaluated the TAB, symmetric QAB (SQAB) and asymmetric QAB (AQAB), considering the active cell FB as the building-block. For the resonant converters, it was adopted similar architecture in order to perform a fair analysis among the MTB topologies. Therefore, it was evaluated the three-port SR (3P-SR), symmetric four-port SR (4P-SSR) and asymmetric four-port SR (4P-ASR) converters. Yet, for the resonant converters, due to their inherent operation characteristics, the bidirectional and unidirectional versions were also considered. In the first case, it was used only the active cell FB (based on SiC MOSFETs, cf. Table VI) to implemented the converters, whereas in the second case, the passive cell FWR (based on SiC schottky diodes) was adopted in the secondary-side cell.

In principle, the same cell might be used as the building block of the non-resonant and resonant converters aforementioned, taking into account the same power rating. However, in

Table V
ELECTRICAL SPECIFICATIONS OF THE MTB DC-DC CONVERTER.

Total Power	Switching Frequency	DC-Link Voltage
$P_{MTB} = 10 \text{ kW}$	$f_{sw} = 20 \text{ kHz}$	$V_{DC,i,j} = 400 \text{ V}$

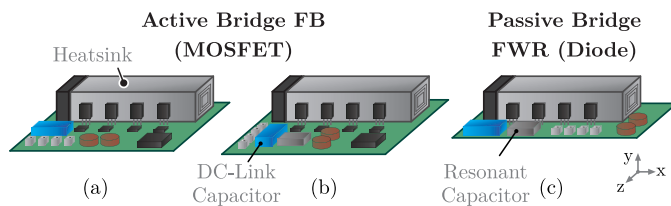


Figure 25. Designed cells used to implement the MTB DC-DC converters for the quantitative analysis, considering the elements described in Table VI and dimensions defined by xyz (width x height y length). The designed cells are used in: (a) the non-resonant MTB converters (150 mm \times 30 mm \times 150 mm); (b) the bidirectional resonant converters (150 mm \times 30 mm \times 160 mm); and (c) secondary-side of the unidirectional 4P-SSR and as the insulated cell of the 3P-SST (150 mm \times 30 mm \times 75 mm). For the insulated cells, the heatsink LAM-3K is replaced by LAM-4K, so that the height is increased to 40 mm.

Table VI
PARAMETERS OF THE MTB CONVERTERS EMPLOYED IN THE QUALITATIVE ANALYSIS.

Selected Devices Main Cells (FB)	SiC MOSFET C3M0060065K - 37 A & 650 V $R_{DS(ON)} = 60.0 \text{ m}\Omega$
Selected Devices Main Cells (FWR)	SiC Diode C3D30065D - 30 A & 650 V
Selected Heatsink Main Cells	LAM-3K - $R_{th} = 1.6 \text{ K/W}$ 30 mm \times 30 mm \times 100 mm
Selected Devices Insulated Cell (FB)	SiC MOSFET C3M0015065K - 120 A & 650 V $R_{DS(ON)} = 15.0 \text{ m}\Omega$
Selected Devices Insulated Cell (FWR)	SiC Diode C5D50065D - 50 A & 650 V
Selected Heatsink Insulated Cell	LAM-4K - $R_{th} = 0.8 \text{ K/W}$ 40 mm \times 40 mm \times 100 mm
Total Leakage Inductance Reactive Network	$L_{k,i,j} = 30 \mu\text{H}$ N27 Ferrite Core E42/21/20 Litz Wire 510 \times 0.1 mm
Resonant Capacitance Reactive Network (only at resonant topologies)	$C_{r,i,j} = 2.2 \mu\text{F}$ MKP385E52240KKP2T0 400 V & ESR = 6.0 m Ω
Multiwinding Transformer	3 parallel cores E80/38/20 Unitary Turn-ration ($a_{i,j} = 1$)

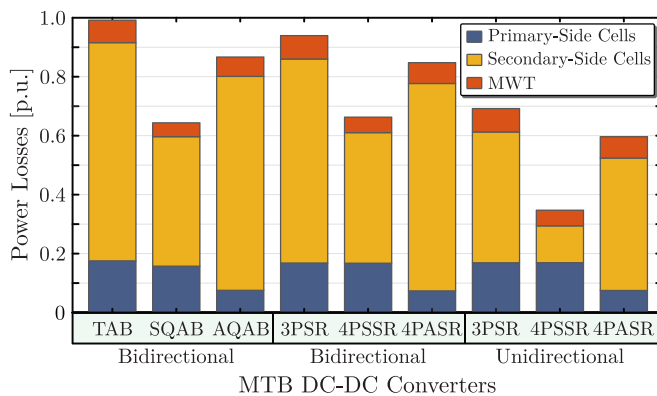


Figure 26. Quantitative Analysis of the MTB topologies in terms of total power losses on the cells (conduction and switching losses) and MWT (ohmic losses), considering the base value equal to 150 W.

Table VII
QUANTITATIVE ANALYSIS OF THE MTB CONVERTERS AT 10 kW, 400 V, 20 kHz AND DIRECT POWER FLOW (PRIMARY TO SECONDARY SIDE).

MTB DC-DC Topologies	Non-Resonant & Bidirectional Active Bridge			Resonant & Bidirectional Series-Resonant			Resonant & Unidirectional Series-Resonant		
	TAB	SQAB	AQAB	3P-SR	4P-SSR	4P-ASR	3P-SR	4P-SSR	4P-ASR
Architecture Symmetry (primary : secondary)	3-Ports (2 : 1)	4-Ports (2 : 2)	4-Ports (3 : 1)	3-Ports (2 : 1)	4-Ports (2 : 2)	4-Ports (3 : 1)	3-Ports (2 : 1)	4-Ports (2 : 2)	4-Ports (3 : 1)
Efficiency [%]	98.27	98.15	98.48	98.36	98.11	98.54	98.73	99.05	98.90
Power Density [W/cm ³]	3.79	3.24	3.02	3.58	3.06	2.85	4.39	3.91	3.33

the following analysis, the resonant capacitor was integrated directly to the cells. As a result, the building-block of the resonant converters are slightly longer than the non-resonant ones, as depicted in Figure 25.

Hence, the results from the quantitative analysis are presented in Table VII and Figure 26. Table VII summarizes the efficiency and power density results, while Figure 26 shows the losses distribution on each investigated MTB topologies. As can be seen, the designed AMTB converters exhibit an superior performance when compared to the symmetrical ones, since the power density is increased without deteriorating the overall efficiency. This is achieved by using the proper selection of the power semiconductors, as discussed in Section III. In relation to the operation mode, both non-resonant and resonant topologies present in general a similar performance from the efficiency and power losses perspective. However, regarding the power density, the resonant topologies can be slightly impacted due to the resonant capacitor, which can increase the volume of their cells, as demonstrated in Table VII.

Finally, the unidirectional resonant MTB converters provide the best efficiency, since the SiC schottky diodes behaves better than the body-diode of the SiC MOSFET. In this application, due to elevated current on the secondary and a direct power flow (i.e. primary-side to secondary-side cells), the current flows simultaneously through the main channel and body-diode of the SiC MOSFETs, so that the conduction losses is highly affected by the forward drop voltage. Consequently, the diode losses on the SiC MOSFET became relevant and should be carefully considered during the selection of the power semiconductor devices.

VI. CONCLUSIONS

The MTB topologies are a promising choice for implementing the isolated DC-DC converters, because they have high performance and economic advantages. In comparison to the modular architectures based on the 2WT, the MTB topologies can reduce the required core material around 10 %, when the MWT is adopted. As a result, this leads to a cost- and size-reduction. Additionally, the usage of AMTB topologies, where multiples cells are placed at the primary side and only one at the secondary side, can further decrease the number of cells and consequently enhance the power density. Therefore,

adopting the MTB topologies instead of the conventional 2WT-based topologies (e.g. multiple DAB and SR converters), the power density can be enlarged by 30 % and the semiconductor device’s cost at least by 15%.

From the availability perspective, the MTB topologies arise with another potential regarding the inherent fault-tolerant capability, which ensures the continuous operation of the system. Thus, in MTB DC-DC converter there are multiple power paths where the processed power can be easily routed the power among the cells, since they are magnetically coupled. Furthermore, since the main cells of the power converter are at the same time the redundant parts that are operating in power-sharing mode, the MWT allows also a cost-reduction avoiding the classic hardware redundancy (extra stand-by cells).

In several application fields, such as EVs, fast charger station, uninterruptible power supply system (UPS), special medicine equipment, more-electric-aircraft (MEA), data processing (and data center), hybrid grids, solid-state transformer (SST) and others; contain at least one DC-DC converter for adapting the voltage and/or control the power processed. Thus, each application imposes different requirements in terms cost, power density, efficiency and reliability. However, these requirements together are conflicting, since the reliability and efficiency can affect directly the cost. Whereas the efficiency is related to the energy saving and a reliable converter to the maintenance cost, the final cost can be also reduced. Therefore, for each application field, one requirement is more critical than the others, which deserves more attention.

In critical application fields with respect to the availability (e.g SST, data center and MEA), the symmetric configuration leads to higher fault-tolerant capability, when compared to the asymmetrical, since the insulated cell can interrupt the power flow when fails. In cost constraint designs, the use of asymmetric MTB architectures has advantages compared to conventional modular two-winding architectures, as the asymmetrical MAB in DC-DC stage of SST applications [18].

For high efficiency applications, the use of non-resonant and resonant MTB DC-DC topologies provide a beneficial trade-off between cost and efficiency when used in asymmetrical configuration. The efficiency of resonant and non-resonant MTB topologies are very similar, only a slight improvement can be obtained in the resonant ones due to the soft-switching wide-range operation [16], [17]. Besides cost and efficiency,

non-resonant MTB converter has enough degree of freedom to control the currents and voltages, contributing to enhance the controllability of the entire system.

Finally, the paper has presented a comprehensive assessment of MTB DC-DC converters, providing information about the potential and challenges for performing resonant and non-resonant MTB topologies in different architectures. Based on these information, a classification and overview of the MTB topologies were done over the paper, highlighting their advantages compared to 2WT. Regarding, the fault-tolerant capability, the MTB DC-DC converter has been presented and evaluated experimentally to validate the multiwinding redundancy approach. As can be seen, the main advantages of the introduced approach are post-fault operation, simple implementation, reduced number of additional components, and no significant efficiency deterioration.

ACKNOWLEDGMENT

This work was supported by the German Federal Ministry for Economic Affairs and Energy (BMWi) within Project KielFlex Kiel als Vorbild für die Errichtung von Ladeinfrastruktur in einem flexiblen Stromnetz zur Umsetzung einer Emissionsreduktion im Transportsektor (01MZ18002D) and also BAEW-project funded by the WTSH and the EKSH of Schleswig-Holstein (LPW-E/1.1.2/1486).

REFERENCES

- [1] M. Liserre, G. Buticchi, M. Andresen, G. De Carne, L. F. Costa, and Z. Zou, "The smart transformer: Impact on the electric grid and technology challenges," *IEEE Ind. Electr. Mag.*, vol. 10, no. 2, pp. 46–58, 2016.
- [2] L. F. Costa, G. De Carne, G. Buticchi, and M. Liserre, "The smart transformer: A solid-state transformer tailored to provide ancillary services to the distribution grid," *IEEE Power Electr. Mag.*, vol. 4, no. 2, pp. 56–67, 2017.
- [3] D. Sha, J. Zhang, and T. Sun, "Multimode control strategy for sic mosfets based semi-dual active bridge dc-dc converter," *IEEE Trans. Power Electr.*, vol. 34, no. 6, pp. 5476–5486, 2019.
- [4] J. Yao, W. Chen, C. Xue, Y. Yuan, and T. Wang, "An isop hybrid dc transformer combining multiple srcs and dab converters to interconnect mvdc and lvdc distribution networks," *IEEE Trans. Power Electr.*, vol. 35, no. 11, pp. 11 442–11 452, 2020.
- [5] Y. Wang, S. Chen, Y. Wang, L. Zhu, Y. Guan, G. Zhang, L. Yang, and Y. Zhang, "A multiple modular isolated dc/dc converter with bidirectional fault handling and efficient ener. conversion for dc distribution network," *IEEE Trans. Power Electr.*, vol. 35, no. 11, pp. 11 502–11 517, 2020.
- [6] H. Matsuo and K. Harada, "New energy-storage dc-dc converter with multiple outputs," *IEEE Trans. Mag.*, vol. 14, no. 5, pp. 1005–1007, 1978.
- [7] Y. M. Chen, Y. C. Liu, and F. Y. Wu, "Multi-input dc/dc converter based on the multiwinding transformer for renewable energy applications," *IEEE Trans. Ind. Appl.*, vol. 38, no. 4, pp. 1096–1104, 2002.
- [8] M. Qiang, W. Wei-yang, and X. Zhen-lin, "A multi-directional power converter for a hybrid renewable ener. distributed generation system with battery storage," in *2006 CES/IEEE 5th Conf.*, vol. 3, 2006, pp. 1–5.
- [9] H. Tao, A. Kotsopoulos, J. L. Duarte, and M. A. M. Hendrix, "Family of multiport bidirectional dc-dc converters," *IEEE Proc. - Electric Power Appl.*, vol. 153, no. 3, pp. 451–458, 2006.
- [10] J. L. Duarte, M. Hendrix, and M. G. Simoes, "Three-port bidirectional converter for hybrid fuel cell systems," *IEEE Trans. Power Electr.*, vol. 22, no. 2, pp. 480–487, 2007.
- [11] S. Inoue and H. Akagi, "A bidirectional isolated dc-dc converter as a core circuit of the next-generation medium-voltage power conversion system," *IEEE Trans. Power Electr.*, vol. 22, no. 2, pp. 535–542, 2007.
- [12] C. Zhao, S. D. Round, and J. W. Kolar, "An isolated three-port bidirectional dc-dc converter with decoupled power flow management," *IEEE Trans. Power Electr.*, vol. 23, no. 5, pp. 2443–2453, 2008.
- [13] S. Falcones, X. Mao, and R. Ayyanar, "Topology comparison for solid state transformer implementation," in *IEEE PES Meet.*, 2010, pp. 1–8.
- [14] S. Falcones, R. Ayyanar, and X. Mao, "A dc-dc multiport-converter-based solid-state transformer integrating distributed generation and storage," *IEEE Trans. on Power Electr.*, vol. 28, no. 5, pp. 2192–2203, 2013.
- [15] L. F. Costa, G. Buticchi, and M. Liserre, "Quad-active-bridge dc-dc converter as cross-link for medium-voltage modular inverters," *IEEE Trans. Ind. Appl.*, vol. 53, no. 2, pp. 1243–1253, 2017.
- [16] L. F. Costa, G. Buticchi, and M. Liserre, "Efficiency/cost trade-off design of a multiple-active-bridge converter for smart transformer," *Conf. Proc. - IEEE Appl. Power Electr. Conf. and Exp. - APEC*, vol. 2018-March, pp. 1163–1170, 2018.
- [17] L. F. Costa, G. Buticchi, and M. Liserre, "Optimum Design of a Multiple-Active-Bridge DC-DC Converter for Smart Transformer," *IEEE Trans. Power Electr.*, vol. 33, no. 12, pp. 10 112–10 121, 2018.
- [18] L. F. Costa, F. Hoffmann, G. Buticchi, and M. Liserre, "Comparative Analysis of Multiple Active Bridge Converters Configurations in Modular Smart Transformer," *IEEE Trans. Ind. Electr.*, vol. 66, no. 1, pp. 191–202, 2019.
- [19] M. A. Rahman, M. R. Islam, K. M. Muttaqi, and D. Sutanto, "A power balance control architecture for multiple active bridge converter in a solidstate transformer," 2020, pp. 1–6.
- [20] S. Bandyopadhyay, P. Purgat, Z. Qin, and P. Bauer, "A multi-active bridge converter with inherently decoupled power flows," *IEEE Trans. Power Electr.*, pp. 1–1, 2020.
- [21] T. G. Wilson, "Cross regulation in an energy-storage dc-to-dc converter with two regulated outputs," in *1977 IEEE Power Electr. Spec. Conf.*, 1977, pp. 190–199.
- [22] H. Matsuo, T. Shigemizu, F. Kurokawa, and N. Watanabe, "Characteristics of the multiple-input dc-dc converter," in *Proc. of IEEE Power Electr. Spec. Conf. - PESC '93*, 1993, pp. 115–120.
- [23] Qing Chen, F. C. Lee, Jian Zhong Jiang, and M. M. Jovanovic, "A new model for multiple-winding transformer," in *Proc. of 1994 Power Electr. Spec. Conf. - PESC'94*, vol. 2, 1994, pp. 864–871 vol.2.
- [24] H. Krishnaswami and N. Mohan, "Three-port series-resonant dc-dc converter to interface renewable ener. sources with bidirectional load and ener. storage ports," *IEEE Trans. Power Electr.*, vol. 24, no. 10, pp. 2289–2297, 2009.
- [25] F. Hoffmann, J.-L. Lafrenz, M. Liserre, and N. Vazquez, "Multiwinding based Semi-Dual Active Bridge Converter," vol. 1, pp. 2142–2149, 2020.
- [26] F. Hoffmann, T. Pereira, and M. Liserre, "Isolated DC/DC Multimode Converter with Ener. Storage Integration for Charging Stations," *IEEE Ener. Convers. Congr. and Exp., ECCE 2020*, pp. 5016–5021, 2020.
- [27] K. Nishimoto, Y. Kado, R. Kasashima, S. Nakagawa, and K. Wada, "Decoupling power flow control system in triple active bridge converter rated at 400 v, 10 kw, and 20 khz," in *2017 IEEE 8th Int. Symp. on Power Electr. for DG Syst. (PEDG)*, 2017, pp. 1–6.
- [28] R. Liu, L. Xu, Y. Kang, Y. Hui, and Y. Li, "Decoupled tab converter with energy storage system for hvdc power system of more electric aircraft," *The Journal of Engineering*, vol. 2018, no. 13, pp. 593–602, 2018.
- [29] R. Rai and N. R. Tummuru, "Circulating and leakage power flow elimination technique between source ports in triple active bridge topology," in *2020 IEEE Int. Conf. (PESGRE2020)*, 2020, pp. 1–6.
- [30] A. Chub, L. F. Costa, and M. Liserre, "Analysis and design of asymmetric QAB converter," *Proc. IECON 2017 - 43rd Annu. Conf. of the IEEE Ind. Electr. Soc.*, vol. 2017-January, pp. 5367–5372, 2017.
- [31] M. A. Rahman, M. R. Islam, K. M. Muttaqi, and D. Sutanto, "Data-driven coordinated control of converters in a smart solid-state transformer for reliable and automated distribution grids," *IEEE Trans. Ind. Appl.*, vol. 56, no. 4, pp. 4532–4542, 2020.
- [32] L. F. Costa, G. Buticchi, and M. Liserre, "Comparison of basic power cells for quad-active-bridge DC-DC converter in smart transformer," *2015 17th European Conf. on Power Electr. and Appl., EPE-ECCE Europe 2015*, vol. 1, 2015.
- [33] G. Buticchi, L. F. Costa, D. Barater, M. Liserre, and E. Dominguez, "A Quadruple Active Bridge converter as the storage interface in the more electric aircraft," *Conf. Proc. - IEEE Appl. Power Electr. Conf. and Exp. - APEC*, vol. 2018-March, pp. 1434–1440, 2018.
- [34] A. El Shafei, S. Ozdemir, N. Altin, G. Jean-Pierre, and A. Nasiri, "Design and implementation of a medium voltage, high power, high frequency four-port transformer," in *2020 IEEE Appl. Power Electr. Conf. and Exp. (APEC)*, 2020, pp. 2352–2357.
- [35] M. A. Rahman, M. R. Islam, K. M. Muttaqi, and D. Sutanto, "Modeling and control of sic-based high-frequency magnetic linked converter for next generation solid state transformers," *IEEE Trans. Ener. Convers.*, vol. 35, no. 1, pp. 549–559, 2020.

- [36] C. Gu, Z. Zheng, L. Xu, K. Wang, and Y. Li, "Modeling and control of a multiport power electronic transformer (pet) for electric traction applications," *IEEE Trans. Power Electr.*, vol. 31, no. 2, pp. 915–927, 2016.
- [37] Y. Tran, D. Dujic, and P. Barrade, "Multiport resonant dc-dc converter," in *IECON 2015 - 41st Annu. Conf. of the IEEE Ind. Electr. Soc.*, 2015, pp. 003 839–003 844.
- [38] Y. Tran, F. D. Freijedo, and D. Dujic, "Open-loop power sharing of three-port dc-dc resonant converters," in *2019 IEEE Appl. Power Electr. Conf. and Exp. (APEC)*, 2019, pp. 2138–2144.
- [39] K. Tomas-Manez, Z. Zhang, and Z. Ouyang, "Multi-port isolated llc resonant converter for distributed energy generation with energy storage," in *2017 IEEE Ener. Conver. Congr. and Exp. (ECCE)*, 2017, pp. 2219–2226.
- [40] W. L. Malan, D. M. Vilathgamuwa, G. R. Walker, and M. Hiller, "A three port resonant solid state transformer with minimized circulating reactive currents in the high frequency link," in *2016 IEEE 2nd Annu. Southern Power Electr. Conf. (SPEC)*, 2016, pp. 1–6.
- [41] Z. Gu, Z. Zheng, and Y. Li, "A power electronic transformer (pet) with multiport bidirectional resonant dc-dc converters for electric traction applications," in *2015 IEEE Trans. Electr. Conf. and Expo (ITEC)*, 2015, pp. 1–6.
- [42] Z. Pavlović, J. A. Oliver, P. Alou, . Garcia, and J. A. Cobos, "Bidirectional multiple port dc/dc transformer based on a series resonant converter," in *2013 Annu. IEEE Applied Power Electr. Conf. and Exp. (APEC)*, 2013, pp. 1075–1082.
- [43] K. T. Manez, Z. Zhang, and Y. Xiao, "Three-port series-resonant converter dc transformer with integrated magnetics for high efficiency operation," in *2018 IEEE Ener. Conver. Cong. and Exp. (ECCE)*, 2018, pp. 5622–5629.
- [44] M. Kazimierczuk, *High-Frequency Magnetic Components*. Wiley, 2011.
- [45] T. Guillod and J. W. Kolar, "Medium-frequency transformer scaling laws: Derivation, verification, and critical analysis," *CPSS Trans. on Power Electr. and Appl.*, vol. 5, no. 1, pp. 18–33, 2020.
- [46] M. Kasper, D. Bortis, and J. W. Kolar, "Scaling and balancing of multicell converters," in *2014 Int. Power Electr. Conf. (ECCE ASIA)*, 2014, pp. 2079–2086.
- [47] V. N. Ferreira, N. Vazquez, B. Cardoso, and M. Liserre, "Hybrid multiple-active bridge for unequal power flow in smart transformers," *2019 IEEE Ener. Conver. Congr. and Exp., ECCE 2019*, pp. 5016–5021, 2019.
- [48] J. Lutz, H. Schlangenotto, and U. Scheuermann, *Semiconductor Power Devices*. Springer, 2011.
- [49] T. A. Pereira, L. Camurca, Y. Ko, R. Zhu, and M. Liserre, "Protection and management of internal faults in modular smart transformer," in *2020 IEEE Appl. Power Electr. Conf. and Exp. (APEC)*, 2020, pp. 1762–1769.
- [50] R. Wu, F. Blaabjerg, H. Wang, M. Liserre, and F. Iannuzzo, "Catastrophic failure and fault-tolerant design of igtb power electronic converters - an overview," in *IECON 2013 - 39th Annu. Conf. of the IEEE Ind. Electr. Soc.*, 2013, pp. 507–513.
- [51] W. Zhang, D. Xu, P. N. Enjeti, H. Li, J. T. Hawke, and H. S. Krishnamoorthy, "Survey on fault-tolerant techniques for power electronic converters," *IEEE Trans. Power Electr.*, vol. 29, no. 12, pp. 6319–6331, 2014.
- [52] M. Andresen, V. Raveendran, G. Buticchi, and M. Liserre, "Lifetime-based power routing in parallel converters for smart transformer application," *IEEE Trans. on Ind. Electr.*, vol. 65, no. 2, pp. 1675–1684, 2018.
- [53] L. F. Costa and M. Liserre, "Failure analysis of the DC-DC converter: A comprehensive survey of faults and solutions for improving reliability," *IEEE Power Electr. Mag.*, vol. 5, no. 4, pp. 42–51, 2018.
- [54] Y. Song and B. Wang, "Survey on reliability of power electronic systems," *IEEE Trans. Power Electr.*, vol. 28, no. 1, pp. 591–604, 2013.
- [55] Q. Xu, Y. Xu, and P. Tu, "Systematic Reliability Modeling and Evaluation for On-Board Power Systems of More Electric Aircrafts," vol. 34, no. 4, pp. 3264–3273, 2019.
- [56] Y. Gou, J. Tian, K. Yu, C. Liu, F. Zhuo, F. Wang, and J. Zhang, "Reliability Modeling and Assessment of Dual Active Bridge Based DC Transformer for DC Power Distribution Application," pp. 6773–6778, 2019.
- [57] V. Raveendran, S. Member, M. Andresen, and M. Liserre, "Improving Onboard Converter Reliability for More Electric Aircraft With Lifetime-Based Control," vol. 66, no. 7, pp. 5787–5796, 2019.
- [58] M. Andresen, K. Ma, G. D. Carne, G. Buticchi, F. Blaabjerg, and M. Liserre, "Thermal Stress Analysis of Medium-Voltage Converters for Smart Transformers," vol. 32, no. 6, pp. 4753–4765, 2017.
- [59] M. Kasper, D. Bortis, G. Deboy, and J. W. Kolar, "Design of a highly efficient (97.7%) and very compact isolated ac–dc telecom power supply module based on the multicell isop converter approach," *IEEE Trans. Power Electr.*, vol. 32, no. 10, pp. 7750–7769, 2017.
- [60] R. Chattopadhyay and S. Bhattacharya, "Decoupled power flow using phase shift control and zvs cases for a three limb high frequency transformer based three-port dab integrating pv and energy storage," in *2016 IEEE Ind. Appl. Soc. Annu. Meeting*, 2016, pp. 1–8.
- [61] D. Hu, D. Ye, Z. Zhang, B. He, and X. Ren, "Optimal design of multi-winding planar transformers in 1 mhz gan multiple-output forward converters," in *2018 IEEE Appl. Power Electr. Confe. and Expo. (APEC)*, 2018, pp. 2288–2293.



Thiago Pereira (S'14) received the B.S. degree in Mechatronics (2011) from the Federal Institute of Santa Catarina (IFSC) in 2011, B.S. and M. S. degrees in electrical engineering from the Power Electronics Institute (INEP) at Federal University of Santa Catarina (UFSC), Florianopolis, SC, Brazil, in 2016 and 2018, respectively. Since 2019, he has been working toward the Ph.D. degree in electrical engineering with the Chair of Power Electronics at Christian-Albrechts-Universität of Kiel, Kiel, Germany. His research interests include DC-DC converters, power converter topologies, reliability in power electronics, high-power converter systems, and wide-bandgap semiconductor devices.



Felix Hoffmann (S'18) received the B.Sc. and M.Sc. degrees in electrical engineering and business administration from Christian-Albrechts-Universität zu Kiel, Kiel, Germany, in 2014 and 2016, respectively. Since 2016, he has been working toward the Ph.D. degree in the Chair of Power Electronics at Christian-Albrechts-Universität zu Kiel, Kiel, Germany. His current research interests include high power converters and the utilization of wide-bandgap semiconductors.



Rongwu Zhu (S'12-M'15) received the B.Eng. in Electrical Engineering from Nanjing Normal University, Nanjing, China, in 2007 and Ph.D. degree in energy technology from Department of Energy Technology, Aalborg University, Aalborg, Denmark, in 2015. From 2011-2012, he was a guest researcher with Aalborg University, and from 2015-2020 he was a senior researcher at Chair of power electronics, at Christian-Albrechts-University of Kiel (Germany). He is currently a full professor at the Harbin Institute of Technology (shenzhen), China.

He has authored and co-authored around 100 technical papers (over 1/3 of them in international peer-reviewed journals/magazine), and 6 patents. His research interests include renewable power generation system, operation and control of electric grid with high penetration of renewables, reliability and resilience improvement of power electronics dominated grid.

He served as a Guest Associate Editor of the IEEE Journal of Emerging and Selected Topics in Power Electronics, Guest Editor-in-Chief of the CSEE Journal of Power and Energy Systems, Editor of the International Transactions on Electrical Energy System, Associate Editor of IEEE Open Journal of Power Electronics, and Technical Committee Chair or Member of several international conferences.



Marco Liserre (S'00-M'02-SM'07-F'13) received the MSc and PhD degree in Electrical Engineering from the Bari Polytechnic, respectively in 1998 and 2002. He has been Associate Professor at Bari Polytechnic and from 2012 Professor in reliable power electronics at Aalborg University (Denmark). From 2013 he is Full Professor and he holds the Chair of Power Electronics at Kiel University (Germany). He has published 500 technical papers (1/3 of them in international peer-reviewed journals) and a book. These works have received more than 35000 cita-

tions. Marco Liserre is listed in ISI Thomson report "The world's most influential scientific minds" from 2014.

He has been awarded with an ERC Consolidator Grant for the project "The Highly Efficient And Reliable smart Transformer (HEART), a new Heart for the Electric Distribution System".

He is member of IAS, PELS, PES and IES. He has been serving all these societies in different capacities. He has received the IES 2009 Early Career Award, the IES 2011 Anthony J. Hornfeck Service Award, the 2014 Dr. Bimal Bose Energy Systems Award, the 2011 Industrial Electronics Magazine best paper award and the Third Prize paper award by the Industrial Power Converter Committee at ECCE 2012, 2012, 2017 IEEE PELS Sustainable Energy Systems Technical Achievement Award and the 2018 IEEE-IES Mittelmann Achievement Award.